TEXTURAL STUDIES OF INTERTIDAL SANDS, BAY OF FUNDY

TEXTURAL STUDIES OF INTERTIDAL SANDS, BAY OF FUNDY

By

CHRISTOPHER ANDREW KASSERRA

A Thesis

Submitted to the Department of Geology

in Partial Fulfilment of the Requirements

for the Degree

Bachelor of Science

McMaster University

April, 1983

BACHELOR OF SCIENCE (1983)
(Geology)

McMASTER UNIVERSITY
Hamilton, Ontario

TITLE: Textural studies of intertidal sands, Bay of Fundy

AUTHOR: Christopher Andrew Kasserra

SUPERVISOR: Professor G.V. Middleton

NUMBER OF PAGES: viii, 76

ABSTRACT

Cobequid Bay is a macrotidal embayment with a large intertidal sand bar complex at the east end, located at the head of the Bay of Fundy. Two sand bars were sampled in order to observe variations in impact pit densities on the surfaces of quartz sand grains, and to identify the pattern of grain size distribution over two intertidal bedforms.

V pit densities obtained by viewing the quartz grain surfaces at magnifications of 10,000 and 5,000X with a scanning electron microscope indicate a linear correlation with grain size. The number of small V's appears to be consistent for all grain sizes, with the result that V's larger than approximately 1/5 micrometer produce the linear variation noted. Two trends of V pits formation combine to produce a "plateau", in which two grain size classes have similar V pit densities. This plateau corresponds to the breakpoint between the traction population and the intermittent suspension population. Trend one consists of the bombardment of large, well exposed grains (transported in the traction layer), by smaller saltating grains, while trend two consists of grain impacts between smaller grains in the concentrated "rheological layer".

Two different grain size patterns were discovered on the two sampled bedforms. A fining upward trend toward the crest on both the stoss and slip faces was observed on an ebb dominated megaripple on Selmah Bar. The exact opposite

pattern was noted on an ebb dominated sandwave from East Noel Bar. On this bedform, an upward coarsening trend toward the crest was discovered on both the stoss and slip faces. These two patterns correspond to the patterns observed by Dalrymple (1977) in his studies of intertidal bedforms.

ACKNOWLEDGEMENTS

I would like to thank Dr. Middleton for suggesting this project and providing the funding and necessary supervision. Special thanks also to Doug Sweeney for his support in helping the author retain a portion of his sanity. I am indebted to Molson Breweries of Canada Ltd. for the use of one of their products,(Brador), which made this last year more enjoyable.

TABLE OF CONTENTS

LIST OF FIGURES

LIST OF TABLES

CHAPTER 1

INTRODUCTION

The Study Area

The Bay of Fundy is located on the east coast of Canada between New Brunswick and Nova Scotia. At its head the bay sub-divides into two smaller branches; Chignecto Bay and Minas Basin-Cobequid Bay (Figure 1.1). Cobequid Bay is found at the eastern tip of Minas Basin, at approximately $45^{o}21'$ N latitude and $63^{o}38'$ W longitude. It is a macro-tidal embayment with a maximum length of forty km and a width of ten km. The tides are semi-diurnal, with a mean range of 11.9 meters at Burntcoat Head (Amos and Long, 1980), which also has the distinction of being the location of the world's largest recorded tidal range (16.3 meters; McWhirter and McWhirter, 1972).

During the periods of low tide, an extensive inter-tidal zone with a width between one-half and five kilometers is exposed along the margin of the bay. Much of this zone is a wave-cut platform which is covered by a thin veneer of gravel and mud along with a few sandbars. As illustrated in figure 1.2, the eastern half of the bay has a large intertidal (and subtidal) sand bar complex that extends across the entire bay.

FIGURE 1.1: Location of the study area (after Dalrymple, 1977)

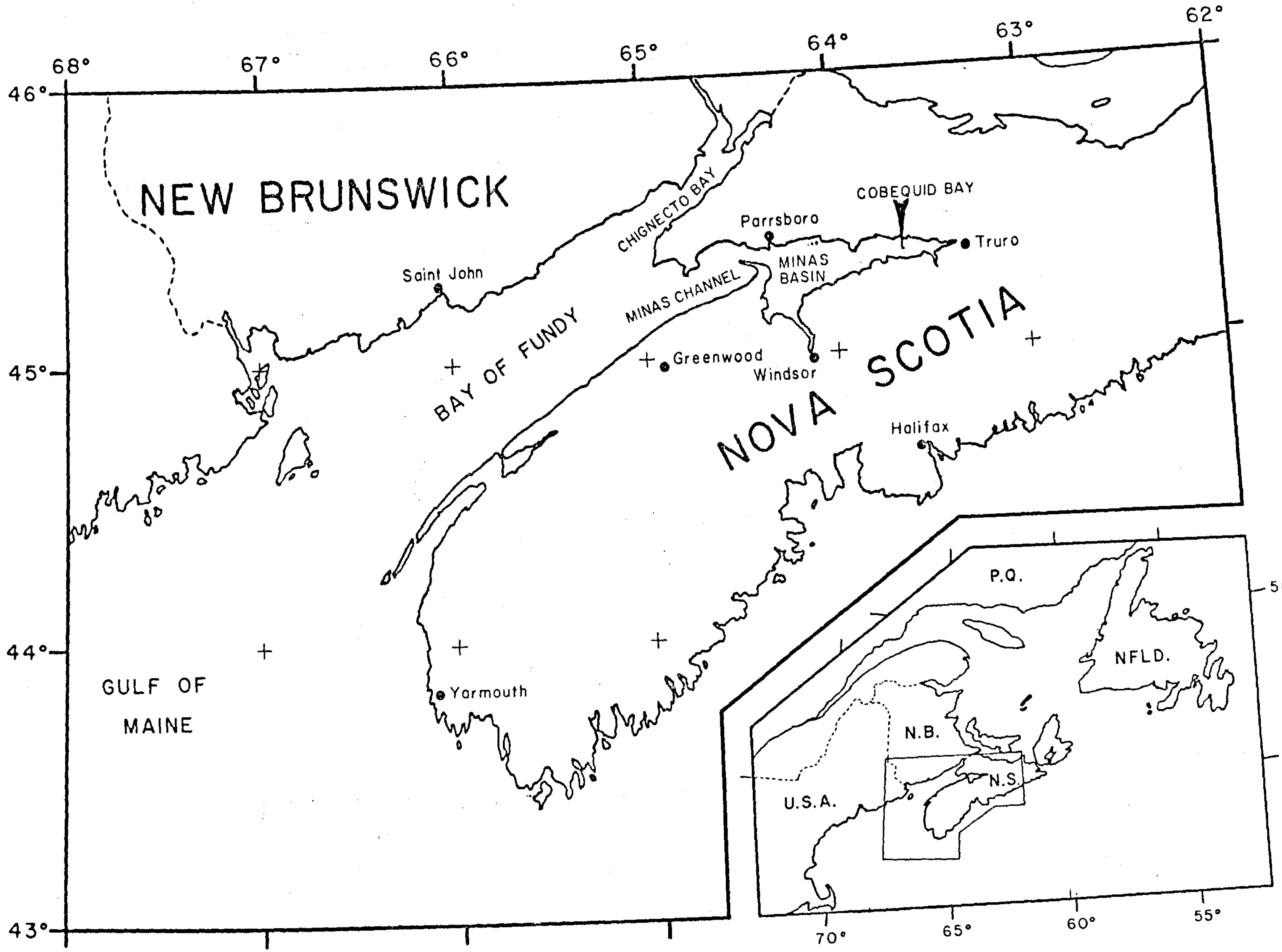

68°
67°
66°
65°
64°
63°
62°
46°
45°
44°
43°
NEW BRUNSWICK
CHIGNECTO BAY
COBEQUID BAY
Parrsboro
Truro
MINAS BASIN
MINAS CHANNEL
Saint John
BAY OF FUNDY
Greenwood
Windsor
NOVA SCOTIA
Halifax
GULF OF MAINE
Yarmouth
P.Q.
NFLD.
N.B.
N.S.
U.S.A.
50°
45°
70°
65°
60°
55°

2

FIGURE 1.2: Cobequid Bay intertidal zone (after Middleton, 1972)

3

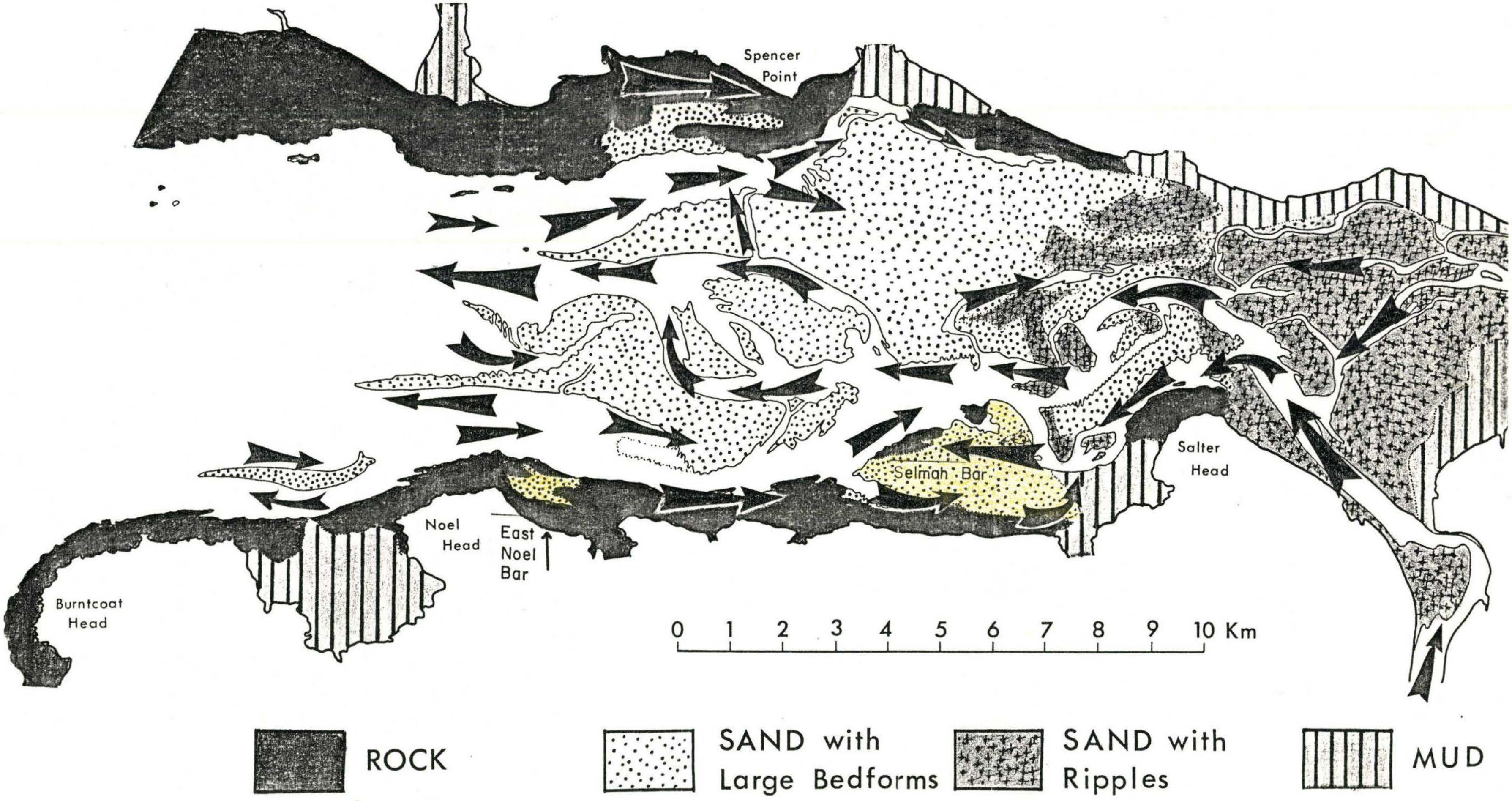

Spencer Point
Salter Head
Selmah Bar
Noel Head
East Noel Bar
Burntcoat Head
0 1 2 3 4 5 6 7 8 9 10 Km
ROCK
SAND with Large Bedforms
SAND with Ripples
MUD

Research Problems

Two different and fundamentally unrelated problems were studied in this project. The first was a study of the variation in grain size distribution over two individual bedforms. The variations were then considered in the light of theoretical studies of fluid mechanics in an attempt to explain them, and to relate the theoretical model with a practical example.

The second problem was a study of impact features on the surface of quartz sand grains. Grain to grain impacts produce among other features, "V" shaped depressions, and the density of these impact pits should relate to the amount of time the grain was near to or on the bed. Complications arise when the age of the grain or the amount of time it has spent in this environment are considered. The density of V pits should be a function of grain size and the velocity of the current, as the larger grains will remain close to the bed while the smaller ones will be able to leap periodically off the bed to form the intermittent suspension population. Higher up in the water column the number of grain collisons will be greatly reduced by the relative scarcity of grains. A simplistic approach would suggest that the inflection point in a cumulative curve (of grain size) between the traction population (C), and the intermittent suspension population (B), should mark the grain size where the trend in the density of V pits should suddenly alter.

Samples from two sides of the sand bar were used in order to detect any differences due to the addition of new material from the shoreline or differences in current velocities. An attempt was also made to correlate the degree of rounding of the sand grains with the density of V pits in order to compare data with Balazs and Kleins' (1972) results which concluded that intertidal processes increased the roundness of the grains. This suggests that the rounder grains should have a higher density of V pits than angular grains.

Geology

The geology of the region surrounding Minas Basin and Cobequid Bay is rather complex, however the area may be subdivided into three broad physiographic regions (Knight, 1977), as demonstrated in figure 1.3. The northern boundary of the Minas Basin-Cobequid Bay area is delineated by the Glooscap fault (Shenk, 1975), which also forms the southern boundary of the Nova Scotia Highlands. The highlands are locally called the Cobequid Mountains. These hills run in an east-west direction and are formed by the Silurian-Devonian Cobequid volcanics complex which was intruded by Devonian granites, and Pennsylvanian sandstones and conglomerates (Dalrymple, 1977).

The Atlantic Uplands form the southern border and a portion of the western edge of the Minas Basin. The uplands

FIGURE 1.3: Geology of the Minas Basin area (after Dalrymple, 1977; Knight, 1977)

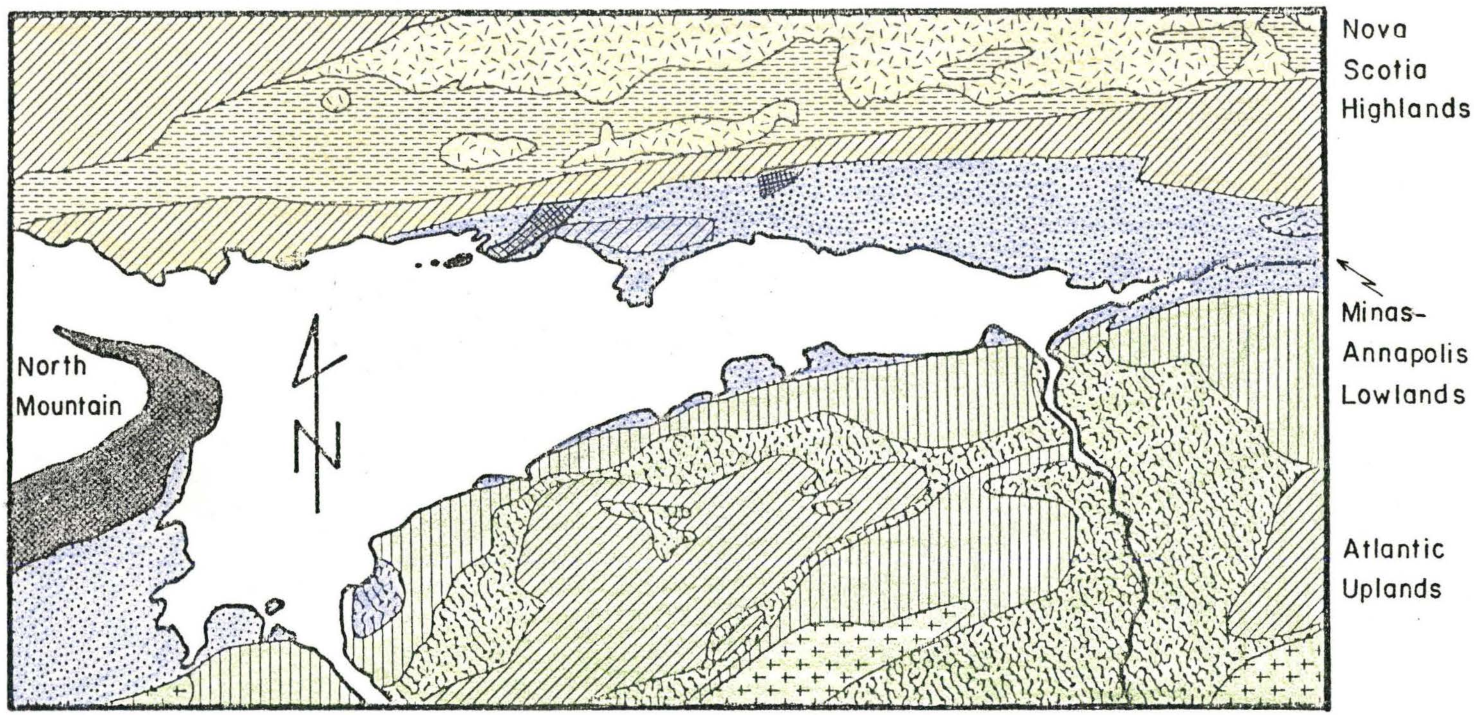

GEOLOGY AROUND THE MINAS BASIN

0 10 20 30 40 km

- Ordovician - Meguma Group shale, siltstone, sandstone
- Silurian & Devonian - Cobequid Complex - volcanics, shale
- Devonian - granite
- Mississippian - Horton Group sandstone, conglomerate, shale
- Mississippian - Windsor Group gypsum, shale, sandstone
- Pennsylvanian - sandstone conglomerate, coal
- Triassic - Annapolis Group sandstone, conglomerate, siltstone
- Triassic - basalt

are mainly Mississippian and Pennsylvanian sandstones, shales and conglomerates with minor exposures in the southern edge of the area of Ordovician sandstones and shales. The western boundary is the North Mountain, which is formed of Triassic basalts, and is also part of the Atlantic Uplands.

The central portion is the Minas-Annapolis Lowlands, which occur on both the eastern and western sides of Minas Basin and Cobequid Bay. These rocks are predominantly Triassic siltstones, sandstones and conglomerates of the Wolfville and Blomidon formations. These rocks form most of the shoreline of both Minas Basin and Cobequid Bay (Klein, 1962), and were deposited as eolian, alluvial fan and lacustrine sediments (Hubert, 1980, 1982). These Triassic sediments are red in color and very friable, and are composed mainly of quartz, but with significant amounts of feldspar and rock fragments in some areas (Klein, 1962).

Glacial History

The last glaciation occurred during the Wisconsin, when a continental ice sheet advanced from the north over the Cobequid Mountains toward the south and southwest (Knight, 1977). A silty, pebbly till was deposited over much of the area, with a thickness that is generally less than 10m (Dalrymple, 1977). Most of the till was derived from local sources, however some distantly derived material is also present.

The ice sheet began to retreat to the north about 13,000 yrs BP. It remained longest in the Cobequid Mountains, producing large amounts of glacial outwash along the north shore. Most of the stream valleys draining down from the mountains toward the north shore were infilled with these sediments. Immediately following the retreat of the ice sheet the sea invaded the Minas Basin, forming a water body into which much of the outwash sediments were deposited as marine deltas.

Isostatic rebound then dominated sea level rise, causing the sea to withdraw. As the rebound slowed, the sea once again began to invade the area around about 5-6000 years ago (Dalrymple, 1977). During the last 4000 years the Bay of Fundy has undergone a slow submergence at a rate (24 cm/100 yrs) faster than eustatic sea level rise (Grant, 1970). This was due in part to isostatic depression of the continental shelf, but mainly to a gradual increase in the tidal range.

The whole Bay of Fundy system may be due to glacial erosion, as suggested by Shepard (1930, 1942), or it may have originated as a result of structural control and fluvial erosion and then been reshaped by the Wisconsin glaciation (Swift and Lyall, 1968).

Sediment Sources

There are four main sediment sources for Minas Basin and Cobequid Bay; coastal erosion, bottom erosion, the Bay of Fundy (via Minas Passage), and fluvial discharge (Amos and Long, 1980). The coastline is predominantly Triassic sedimentary rock, Pleistocene tills and glacio-fluvial sediments, all of which are very easily eroded. The similarity in color and lithology between the intertidal sediments and the shoreline sources, along with an estimated mean cliff recession rate of 0.55 m/year (Amos and Long, 1980), suggest the importance of coastal erosion as a major sediment source. Cobequid Bay itself receives approximately 0.38 x $10^6 m^3$ of sediment annually from this source alone.

Bottom erosion at present does not supply new sediment, it merely reworks and distributes material already in the system (Knight, 1977; Amos and Long, 1980). However, it is very likely that during the formation and growth of Minas Basin and Cobequid Bay (after deglaciation), the bottom erosion and reworking of glacial sediments and soft Triassic rock could have supplied much of the present-day intertidal sediments (Knight, 1977).

Sediment is transported through the Minas passage in suspension, with a minor net residual into Minas Basin. The three main rivers entering the Minas Basin-Cobequid Bay system are the Avon, Salmon and Shubenacadie. They are relatively small, with low discharges and suspended sediment concentrations, and thus do not contribute much sediment (Knight, 1977).

CHAPTER 2

FIELD WORK

Field work was carried out on two intertidal sand bars; Selmah Bar and East Noel Bar (see figure 1.2). Selmah Bar is a large sand bar about four kilometers long and between one and two kilometers wide, located just off the south shore of Cobequid Bay. The sand has a general thickness of less than 5m (Knight, 1977), and a mean grain size that varies from one phi on the southern side to two phi on the northern edge. The sand bar surface has a complete hierarchy of bedforms, ranging from ripples and megaripples to sandwaves. Selmah Bar has existed in the same general location since at least 1860 (date of first available chart), although numerous changes have been observed since 1938 when the first air photos were taken (Dalrymple, 1977). This would indicate that the bar is a semi-equilibrium form, and may be a long term feature.

Samples were taken from stations SB-I and SB-MIII, on opposite sides of the sand bar (figure 2.1). Station SB-I was located in the middle of the stoss side of a large flood dominated sand wave, with a wavelength of 38.8m and an amplitude of 0.67m. The sand wave had sinuous megaripples superimposed on the stoss side, with wavelengths of 1.4m

FIGURE 2.1: Selmah Bar

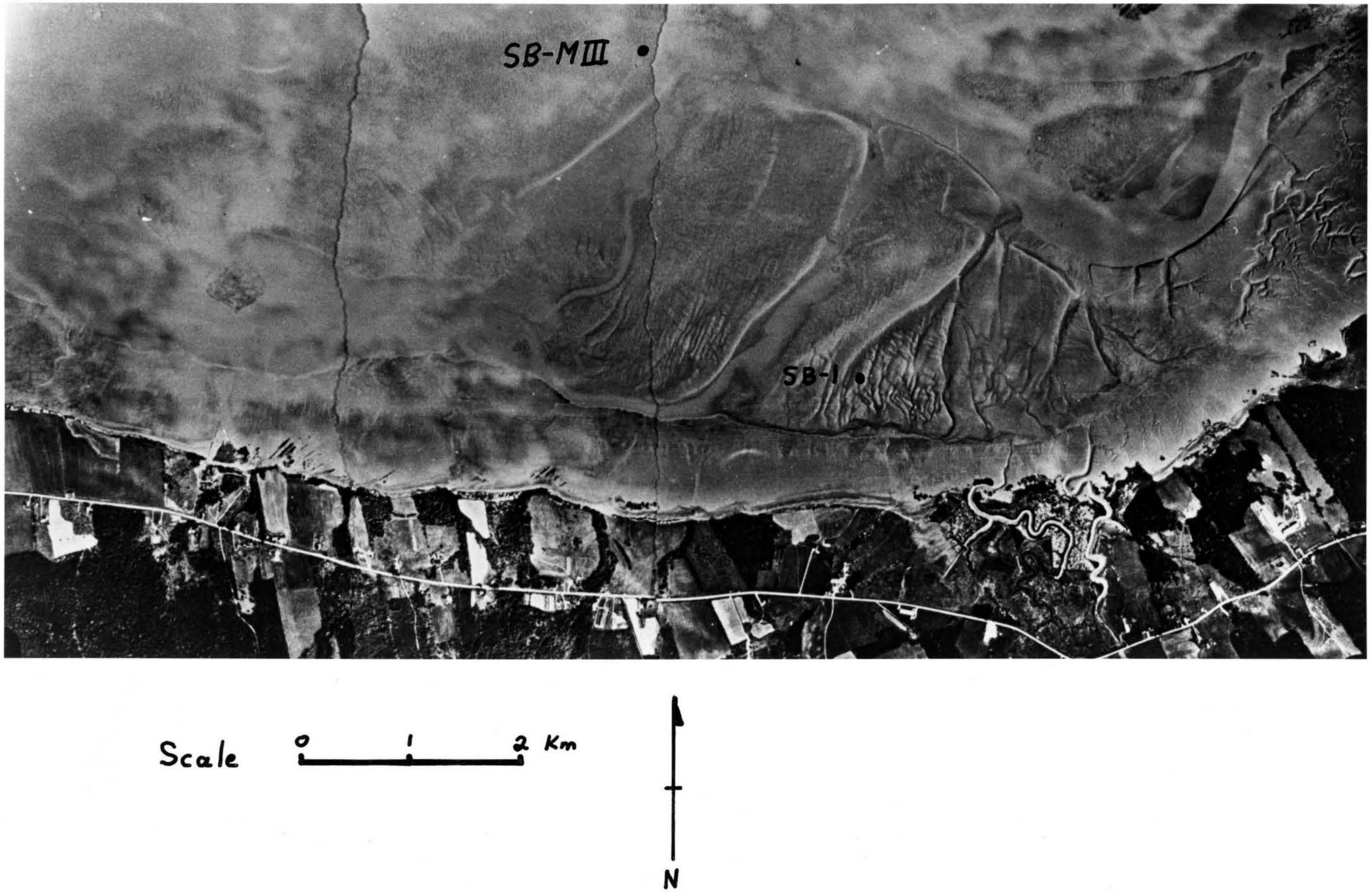
SB-MIII
SB-1
Scale
0
1
2 Km
N

and amplitudes of 15cm. Two samples were collected, one from the crest and another from the trough of a megaripple. Station SB-MIII was located in the center of a field of ebb dominated sinuous type II megaripples. A single megaripple with a wavelength of 6.17m and an amplitude of 0.76m was sampled along two transects perpendicular to the crest line. (See figure 2.2). Samples were taken at 50cm intervals down the stoss side and at 15 cm intervals down the slip face.

The stoss side slope changed from 10^{o} near the crest to 23^{o} at the trough. The slip face was angle of repose, with a slope of 30^{o}. The stoss side had numerous small sinuous current ripples superimposed on it. These ripples are formed during the final few minutes of the ebb as the current speed passes through the ripple stability field (Dalrymple, 1977). The orientation of the crestlines of these ripples with respect to that of the megaripple varied from 1^{o} near the crest to a maximum of 20^{o} at the trough. This is due to increasing channelization of water along the trough of the megaripple as the water level falls below the level of the megaripple crest.

For this study the orientation of the ripples had to be almost parallel to the megaripple crestline in order to best preserve the grain size distribution of the original megaripple surface. If the ripples were oriented at a substantially different angle, they would indicate sediment transport in a different direction than that which supplied

FIGURE 2.2: Sample location SB-MIII on Selmah Bar.

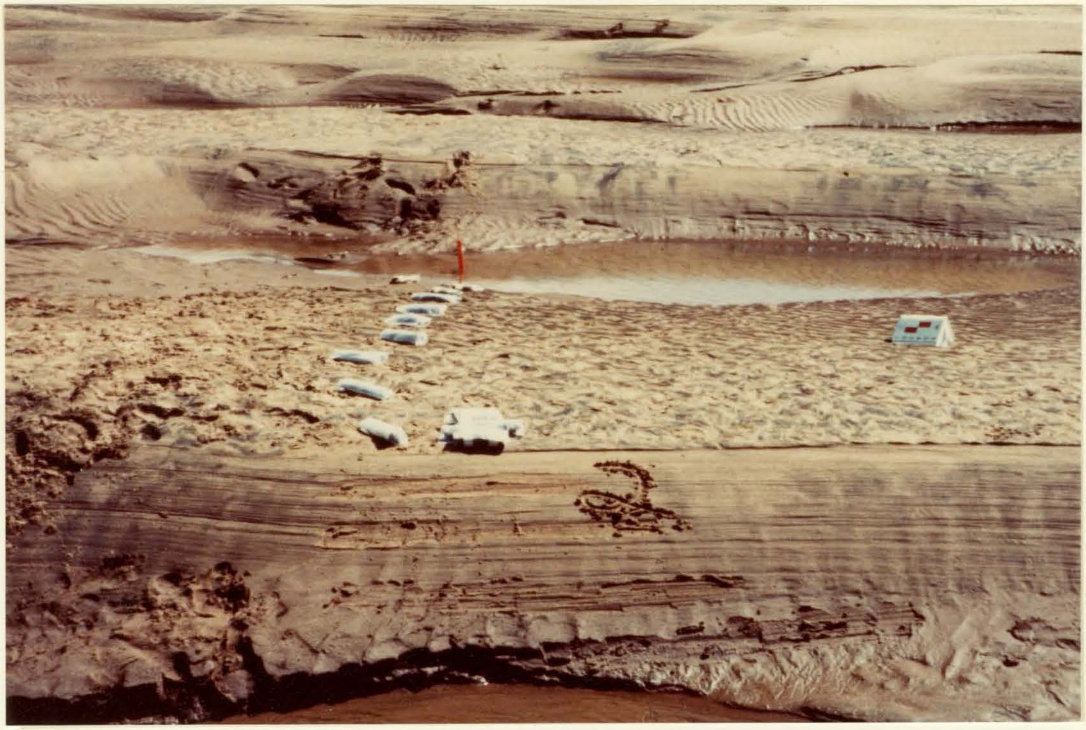

the megaripple. These ripples would have the effect of disturbing the top few centimeters of sediment and transporting the finer grains only, due to the lower current velocity.

East Noel Bar is a small sand bar about 1.3 kilometers long and 0.5 kilometers wide located in the lee of Noel Head on the south shore of Cobequid Bay (See figure 2.3). The sand body has a general thickness of less than 2m (Dalrymple, 1977), and a mean grain size of 2.3 phi at the sample location. An ebb dominated, rippledsand wave with a wavelength of 17.2m and an amplitude of 0.61m was intensively sampled at site ENB along a transect perpendicular to the crest line.

Samples were taken at 1m intervals along the stoss side, with sample ENB-1p at the base of the slipface of the next sandwave. Samples were taken down the slip face at 10cm intervals (See figure 2.4). The stoss side slope was an average of 3°, while the slip face had a slope of 28°. The samples were obtained by scraping up the top one to two cm of sand until a sample of 200-250 grams was obtained. All samples included sand from both the troughs and crests of the samll superimposed ripples in order to minimize differences due to sorting in the ripples themselves.

Sample Preparation

The two samples from the trough and crest of a mega-

FIGURE 2.3: East Noel Bar

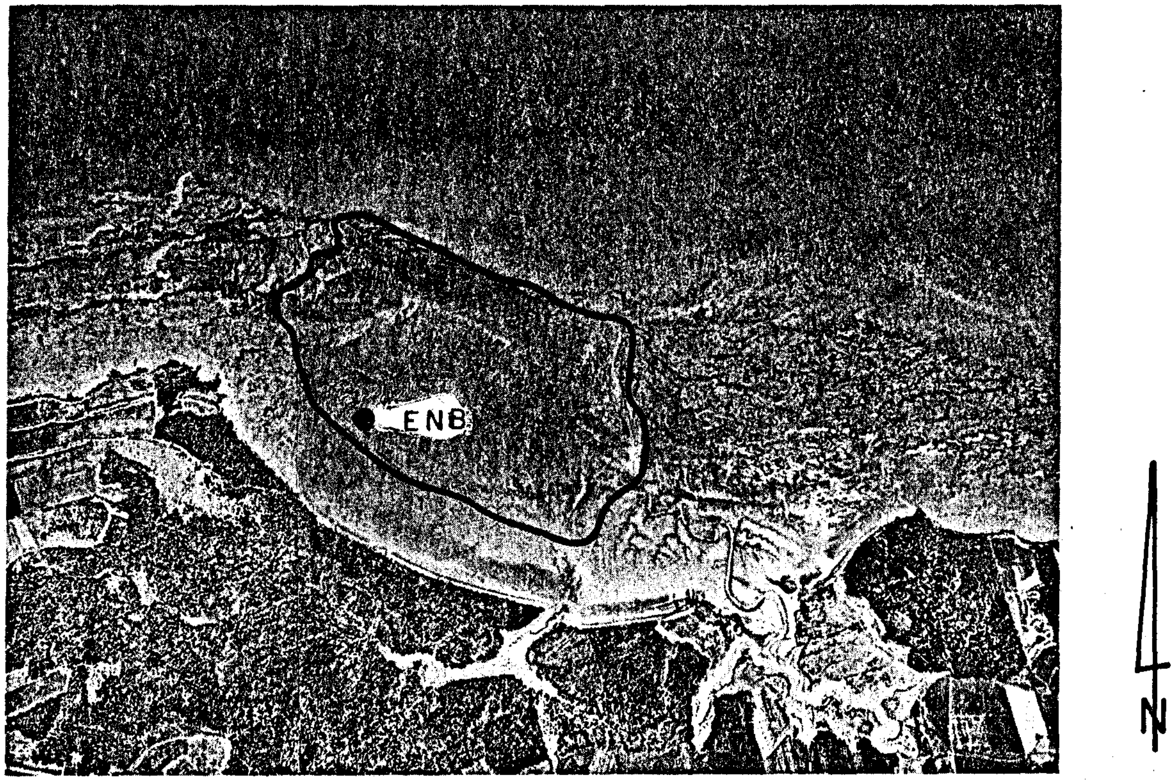

1973 EAST NOEL BAR

SCALE 0 1 2 km

FIGURE 2.4: Sample location ENB on East Noel Bar

ripple at station SB-I, and fourteen samples from transect line two of station SB-MIII on Selmah Bar, along with fifteen samples from transect line one of station ENB on East Noel Bar were used in this study.

The initial sample preparation was very similar to that described by Dickson (1974). The field samples were in the range of 200 to 250 grams, and thus were too large to sieve accurately. The samples were first oven dried at 40°C, and then gently disaggegated with a rubber pestle. The samples were then split in a riffle into subsamples of between 30 and 70 grams in size, as suggested by Folk (1980). The subsamples were placed on a four phi sieve and washed with three liters of distilled water in order to remove the soluble salts and silts and clays. Initially the weight of the silt and clay fraction was determined by filtering the wash water. However the amount of fines present in most of the samples was very low (less than 0.6%), which is in agreement with Dalrymples'(1977) findings. As a result the filtering was discontinued, as the exact percentage of fines is not important to this study.

After washing, the subsamples were oven dried and sieved. The sieves used ranged from -1.5 phi to +4.0 phi at 0.5 phi intervals. The samples were shaken on the Ro-tap machine for ten minutes, and each size fraction was then weighed using a Mettler balance.

Grains for use with the Scanning Electron Microscope (SEM) were taken from station SB-MIII, sample C-2 (for location see figure 5.1) and station SB-I, megaripple trough sample. These samples were used due to the greater abundance of larger grains.

The sample preparation method is similar to that of Krinsley and Doornkamp (1973) and Davis (1978). Approximately fifty quartz grains from each sieved size fraction were randomly collected and placed on a black gridded microscope slide with the use of a fine paint brush. The slide was then systematically scanned, removing every second or third grain until fifteen to twenty grains were assembled. These grains were observed under a binocular microscope, and unsuitable grains were rejected. They were then placed in a 50ml beaker containing a stannous chloride solution and boiled for twenty minutes. Following this they were rinsed in distilled water and then boiled in distilled water for ten minutes to remove adhering crystals of stannous chloride. The grains were then placed in 40ml of concentrated hydrochloric acid and boiled for twenty minutes to remove any surface debris and then rinsed again with distilled water.

This sequence of solutions is opposite to that of Krinsley and Doornkamp (1973), who suggest that first HCl and then stannous chloride solutions be used. The drawback to this is that if a more concentrated solution of stannous chloride is used, washing with distilled water will not remove the crystals of stannous chloride that form in the microdepressions and pits on the grain surface. Thus collision V pits and other small features may be obscurred, as shown in figure 2.5. A reversal of the solution sequence allows two cleansing baths, first in distilled water and then in HCl to remove the adhering crystals.

When dry, the grains were mounted on aluminum SEM stubs coated with Scotch Brand double coated conductive tape No. 410, 3M Company (Davis, 1978). When the fifteen to twenty grains had been placed on the stub, a reference map of the stub surface was drawn to aid identification during SEM viewing (Davis, 1978). The stub was viewed under a binocular microscope and the grains were classed according to Power's roundness scale (AAPG Memoir 28, pg. 102). Each stub was then coated with a 200 Angstrom thick layer of gold alloy in a vacuum evaporater, to avoid a charge build up during viewing with the SEM. The SEM used was a Philips SEM 501, and photographs were taken with Kodak 400ASA TX 135 black and white film.

Figure 2.5: Adhering crystals of stannous chloride

a - Magnification = 5000X

Scale bar equals one micrometer

b - Magnification = 10000X

Scale bar equals one micrometer

a

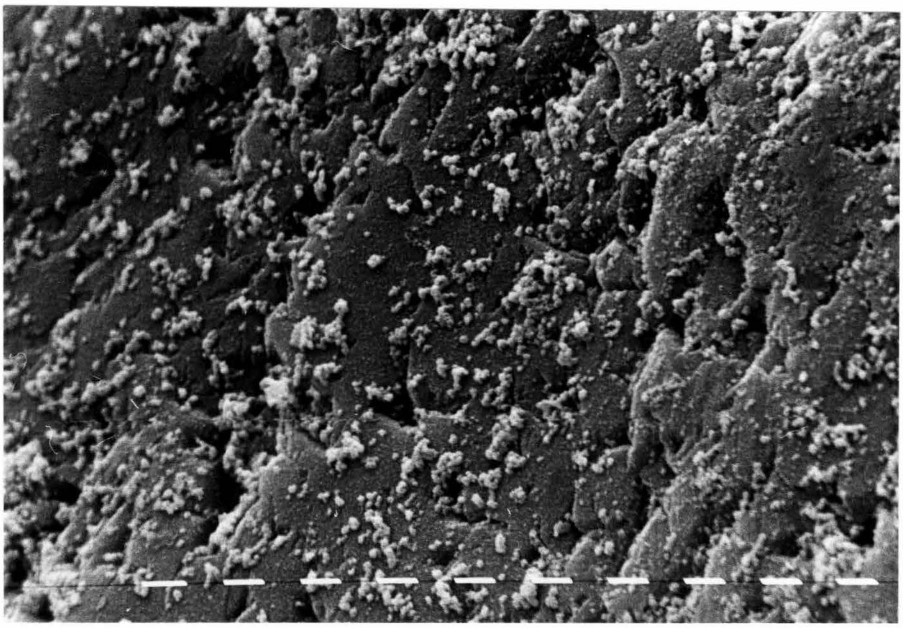

b

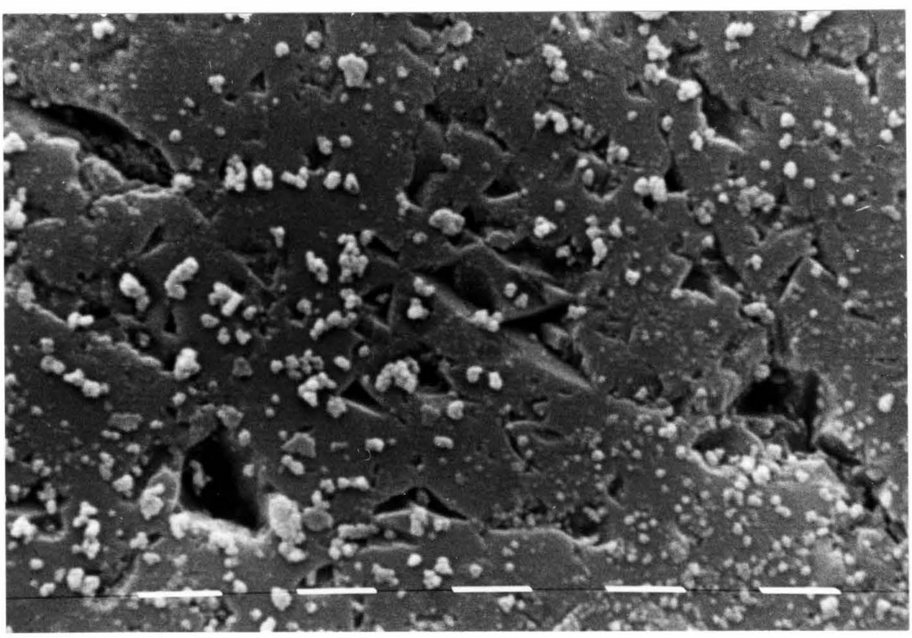

Chapter 3

Literature Review

Mechanical collison features or "V" pits had been recognized by 1962, and it was in 1964 that Krinsley, Takahashi, Silberman and Newman published the first paper with an in-depth study of V pitting. They concluded that the density of V pits on beach sand grains was related to the distance the grains had travelled from their source.

In 1968 Krinsley and Donahue continued this research with a more detailed analysis of V shaped patterns on beach sand. They found it possible to distinguish high, medium and low energy beach environments. Low energy beach grains contain en echelon, oriented V shapes, thought to be due to chemical etching. As wave energy increases, the size and number of randomly oriented V's increases, and dominates the etch pits. They discovered that on some photographs the mechanical V pits were not randomly oriented, as in many cases, but that sets with a certain orientation pattern could be seen. They postulated that a set of oriented V pits could be the result of a single collision, where the protuberances on one grain abrade the other grain with a linear motion. Krinsley and Smalley (1972) also noted irregular, partially oriented V pits which they thought were due to orientation along a dominant cleavage; however, they also always observed more than one main orientation direction.

Margolis (1968) agreed with Krinsley's results in that the number of chemical and mechanical features on quartz beach grains could be correlated with wave energy conditions. He also experimentally etched quartz grains to produce chemical V shapes, and concluded that the best etching would occur in solutions with a pH greater than 9. Such a high pH could be formed on beach or intertidal areas exposed to periodic drying. The evaporation of the water film surrounding the quartz grain would produce the necessary alkaline conditions.

In 1969, the first studies using an SEM (instead of a TEM) to observe sand grains were published (Krinsley, Steiglitz). It was rapidly discovered that although the resolution of the SEM was much poorer than the TEM, the rapid processing of samples, great depth of field and realistic photographs of the grains themselves would allow much more accurate work to be done.

Margolis and Kennett (1971) concluded that it was possible to differentiate between deep-sea turbidites and river, beach and shallow water turbidites on the basis of V pit densities. An experimental, artificial saturation limit for V pit densities was determined to be about 6.5 per square micron, due to the observation that further pitting would erase pre-existing ones. They also found that pit densities increased with an increase in the percent of grains developing significant pitting (figure 5.11). This supports previous studies (Krinsley _et_ _al_., 1964; Krinsley _et_ _al_., 1968; Margolis, 1968) that the formation of subaqueous mechanical V pits is a function of the (turbulent) energy of the environment.

Blackwelder and Pilkey (1971) discovered that the mineralogy of the beach or shelf sand may have an effect on V pitting. Six samples from shelf areas south of Cape Romain, South Carolina, exhibited predominantly solution features, with only minor evidence of beach modification in the form of V pitting. They suggested that the high calcium carbonate content of sediment of the area may have reduced quartz to quartz grain impacts, with the effect of exaggerating the solution etch pits.

In 1973 Krinsley and Doornkamp published what has become the standard reference for quartz grain microtextures. They summarized all of the knowledge on quartz surface textures up to that time, and defined various environments and textures using the best "classical" photographs available.

Wehrfritz (1973) observed a number of quartz grains from an intertidal zone and concluded that the frequency of V shapes increased on grains of increasing roundness. However he noted that this may be due to the fact that angular grains with many low protected areas would not have as many features due to the lower surface area available for impacts.

In 1974, Ingersoll published one of the very few papers on first cycle sand grains. He examined beach sands derived from local granitic rocks and found only those textures described from other high energy beach environments, thus providing reassurance that these features are indeed diagnostic. He also noted that all investigators tended to indicate that chemical textures were relatively more common on smaller grains, while mechanical features were relatively more common on larger grains.

The crystallographic properties of quartz were for the first time related to the physical and chemical mechanisms that produce the microfeatures on quartz grain surfaces by Margolis and Krinsley (1974).

Hampton <u>et al</u>. (1978) published the first study on quartz grain microtextures from a large tidal estuary. Samples from a large sand wave field in water depths of 50 to 100 meters had numerous mechanical impact features. Grain velocities in the order of 30 cm/sec were noted over the crests of the bedforms, providing the required high energy environment. This study, along with Margolis's(1968), indicates that V pits are not indicative of only beach environments, but also any higher energy, sandy environment.

Middleton and Davis (1979) discussed the effects of high turbulence on the abundance of mechanical impact features. They noted that the important factors in determining the amount of mechanical attrition are the number and intensity of grain impacts. This may depend on more than the level of turbulence, and factors such as the size of the grains and the density of the "sand cloud" in suspension may be very important.

A great majority of the articles published on quartz grain microtextures mention V pitting in a very qualitative manner. Few authors actually include quantitative values, and none have studied the variation in density or size of V pitting on grains of different sizes. A large part of this study is an attempt to detect any changes in V pit densities that may be due to differences in the size of the grains, and hence their particular mode of transporation in the subaqueous environment.

Chapter 4

Grain Size Variation Over Bedforms

Two bedforms were sampled at close intervals down both the stoss and lee faces, in order to determine the variation in the grain size distribution. Both bedforms chosen were ebb dominated, in order that they should show the least modification of the dominant bedform morphology at low tide, which was the only period the sand body was accessible. Samples SB-MIII were taken from a megaripple on Selmah Bar, while samples ENB were scraped from a rippled sand wave on East Noel Bar (For locations see figures 2.1 and 2.3).

A rough sketch of the individual sample locations on the bedforms is shown in figure 4.1. The sampling methods and intervals and the bedform measurements are discussed in Chapter 2. The basic sieve data in the form of cumulative weight percent for all samples analysed is located in appendix 2.

For each sample from the two bedforms, summary statistics were calculated and plotted in figures 4.2, 4.3, 4.4 and 4.5. Graphic mean, inclusive graphic standard deviation, inclusive graphic skewness and graphic kurtosis as defined by Folk (1980) were calculated from cumulative curves drawn for each sample. The graphic mean was always

FIGURE 4.1: Diagramatic representation of bedform and sample locations

Samples SB-MIII
see also figure 2.2

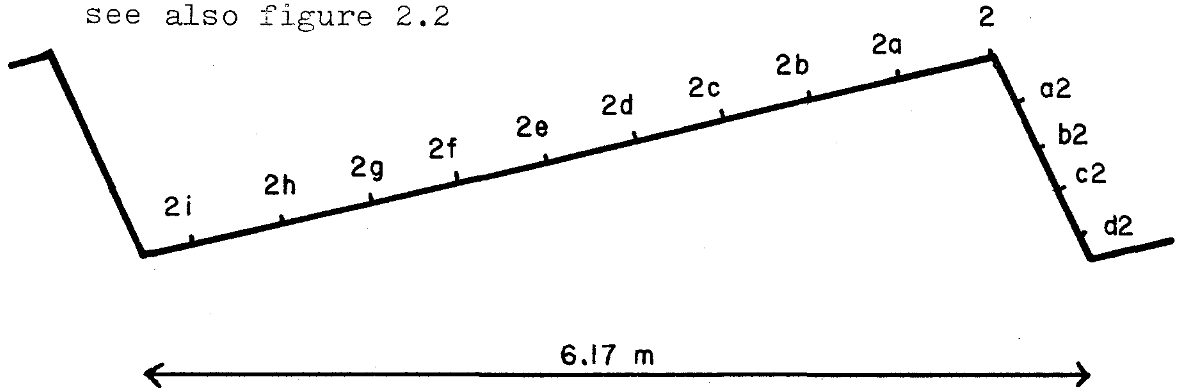

Samples ENB
see also figure 2.4

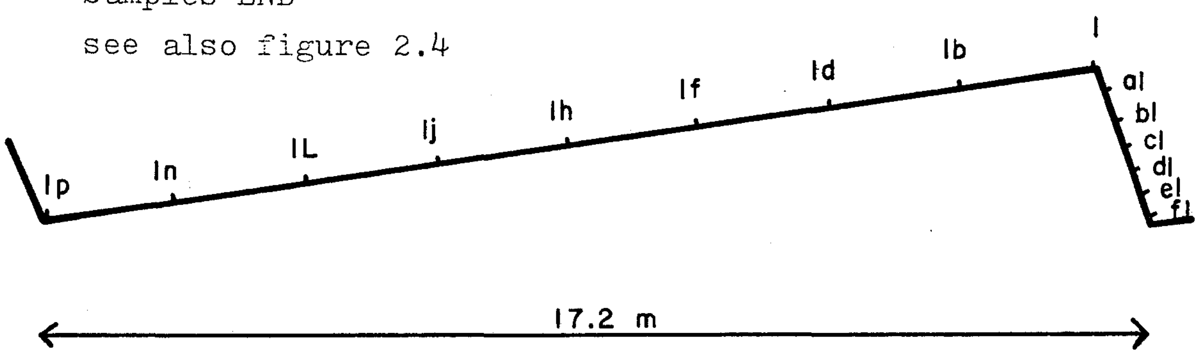

checked with the results of a calculator program which used the method of moments as outlined by Seward-Thompson and Hails (1973). The two methods gave results which never varied by more than 0.02 phi units from each other.

Linear regression by the method of least squares was applied to each of the data sets in figures 4.2 through 4.5. The correlation coefficient, r^2, measures goodness of fit of the data points to the regression line. The r^2 value will always lie between zero and one, and the closer it is to one, the better the fit.

The bedforms exhibit two distinctly different patterns of grain size variation which are similar to the two patterns noted by Dalrymple (1977) in his studies of intertidal bedforms. Dalrymple used 77 samples taken from 20 different locations and discovered that the type of grain size pattern appeared to depend on whether the bedform had an avalanche face or not. In this study, 29 samples from 2 locations were examined to test Dalrymple's results.

Dalrymple's (1977) pattern type one was found on the megaripple at SB-MIII. The main feature of this pattern is the concentration of coarser material at the lower portions of both the stoss and slip faces. This is indicated in figures 4.2a and 4.3a by the coarsening trends away from the crest. The coarsening of the mean grain size on the stoss side toward the trough is most likely due to the increase in average shear stress from the trough to the crest. This

FIGURE 4.2: Variation in grain summary statistics on the stoss slope of megaripple SB-MIII.

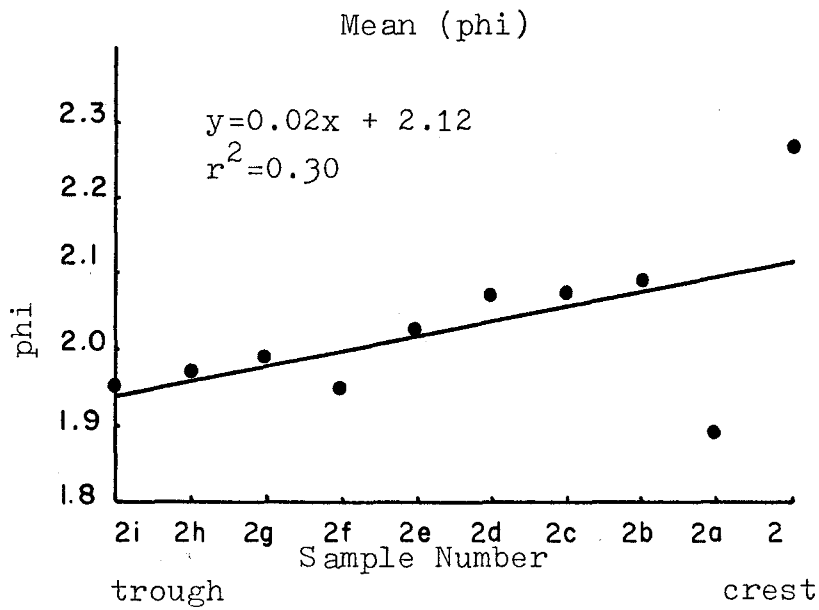

Mean (phi)
y=0.02x + 2.12
r2=0.30
phi
2.3
2.2
2.1
2.0
1.9
1.8
2i 2h 2g 2f 2e 2d 2c 2b 2a 2
Sample Number
trough
crest

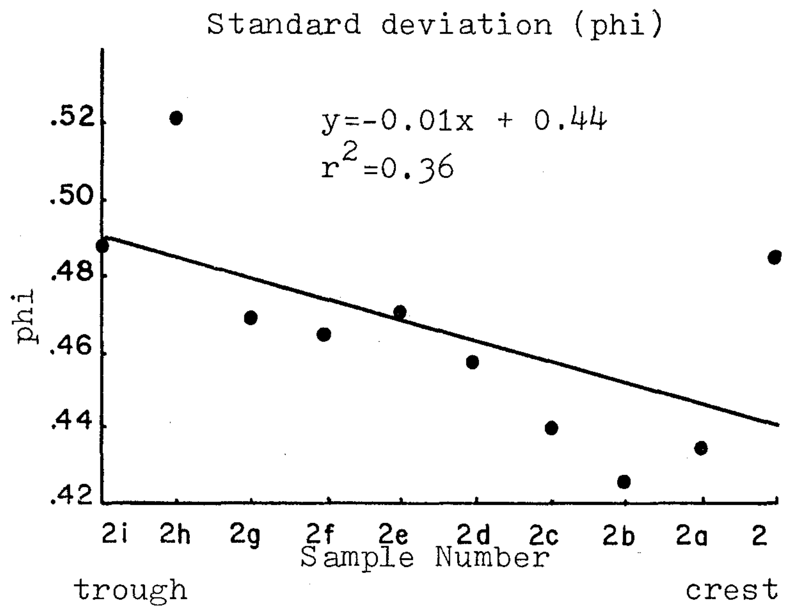

Standard deviation (phi)
y=-0.01x + 0.44
r2=0.36
phi
.52
.50
.48
.46
.44
.42
2i 2h 2g 2f 2e 2d 2c 2b 2a 2
Sample Number
trough
crest

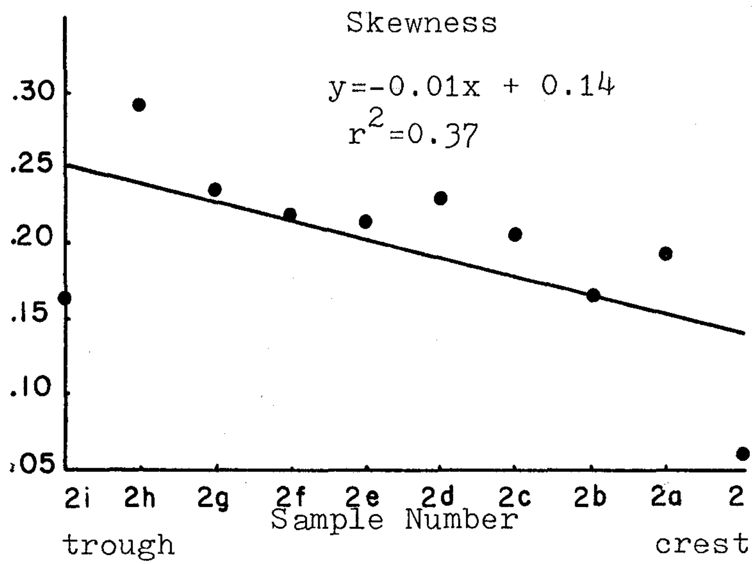

Skewness
y=-0.01x + 0.14
r2=0.37
.30
.25
.20
.15
.10
.05
2i 2h 2g 2f 2e 2d 2c 2b 2a 2
Sample Number
trough
crest

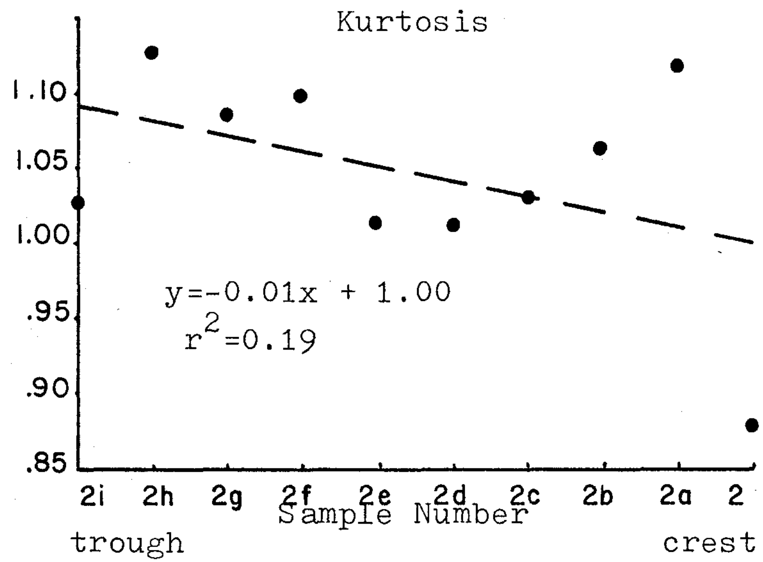

Kurtosis
y=-0.01x + 1.00
r2=0.19
1.10
1.05
1.00
.95
.90
.85
2i 2h 2g 2f 2e 2d 2c 2b 2a 2
Sample Number
trough
crest

FIGURE 4.3: Variation in grain summary statistics on the slip face of megaripple SB-MIII

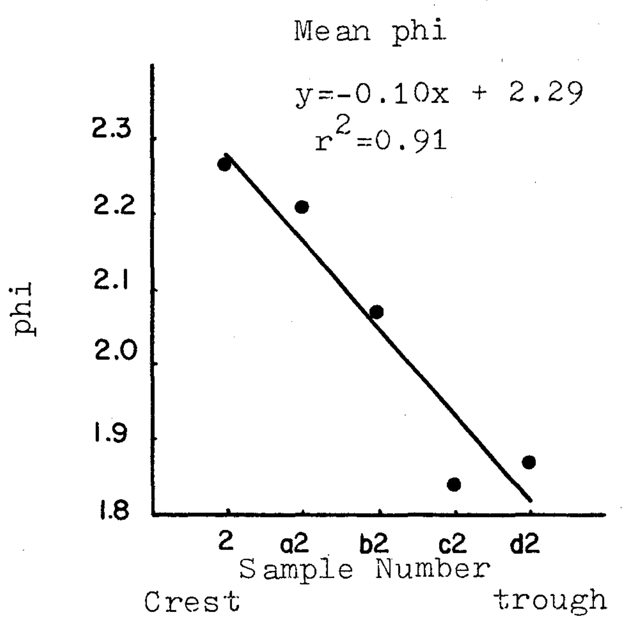
Mean phi
y=-0.10x + 2.29
r^2=0.91
2.3
2.2
2.1
2.0
1.9
1.8
phi
2
a2
b2
c2
d2
Sample Number
Crest
trough

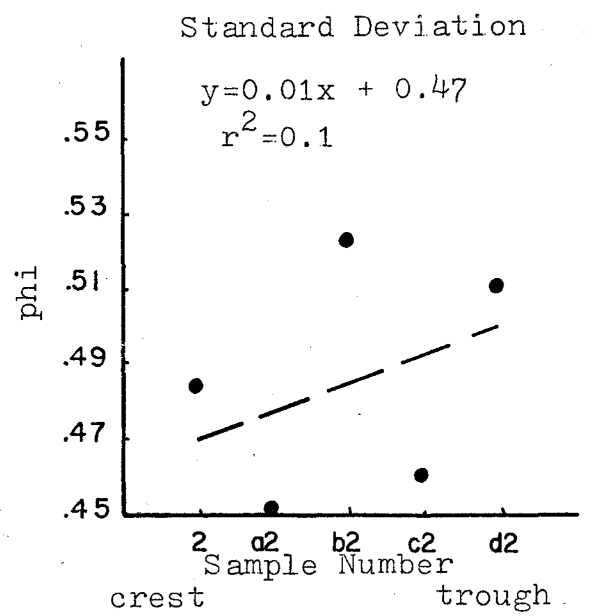
Standard Deviation
y=0.01x + 0.47
r^2=0.1
.55
.53
.51
.49
.47
.45
phi
2
a2
b2
c2
d2
Sample Number
crest
trough

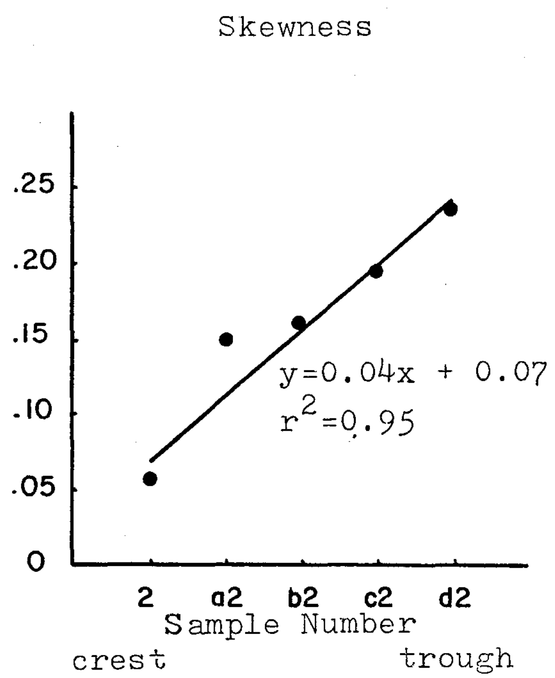
Skewness
.25
.20
.15
.10
.05
0
y=0.04x + 0.07
r^2=0.95
2
a2
b2
c2
d2
Sample Number
crest
trough

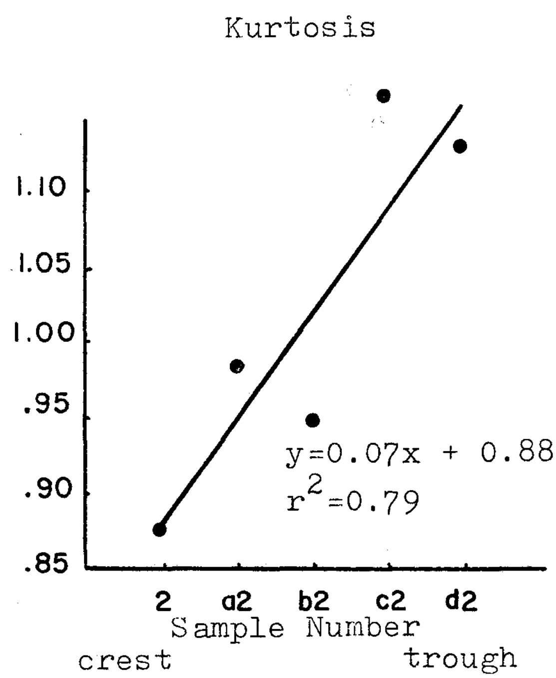
Kurtosis
1.10
1.05
1.00
.95
.90
.85
y=0.07x + 0.88
r^2=0.79
2
a2
b2
c2
d2
Sample Number
crest
trough

FIGURE 4.4: Variation in grain summary statistics on the stoss slope of sandwave ENB (Value for 1_p is not included as it representes the base of the next slipface)

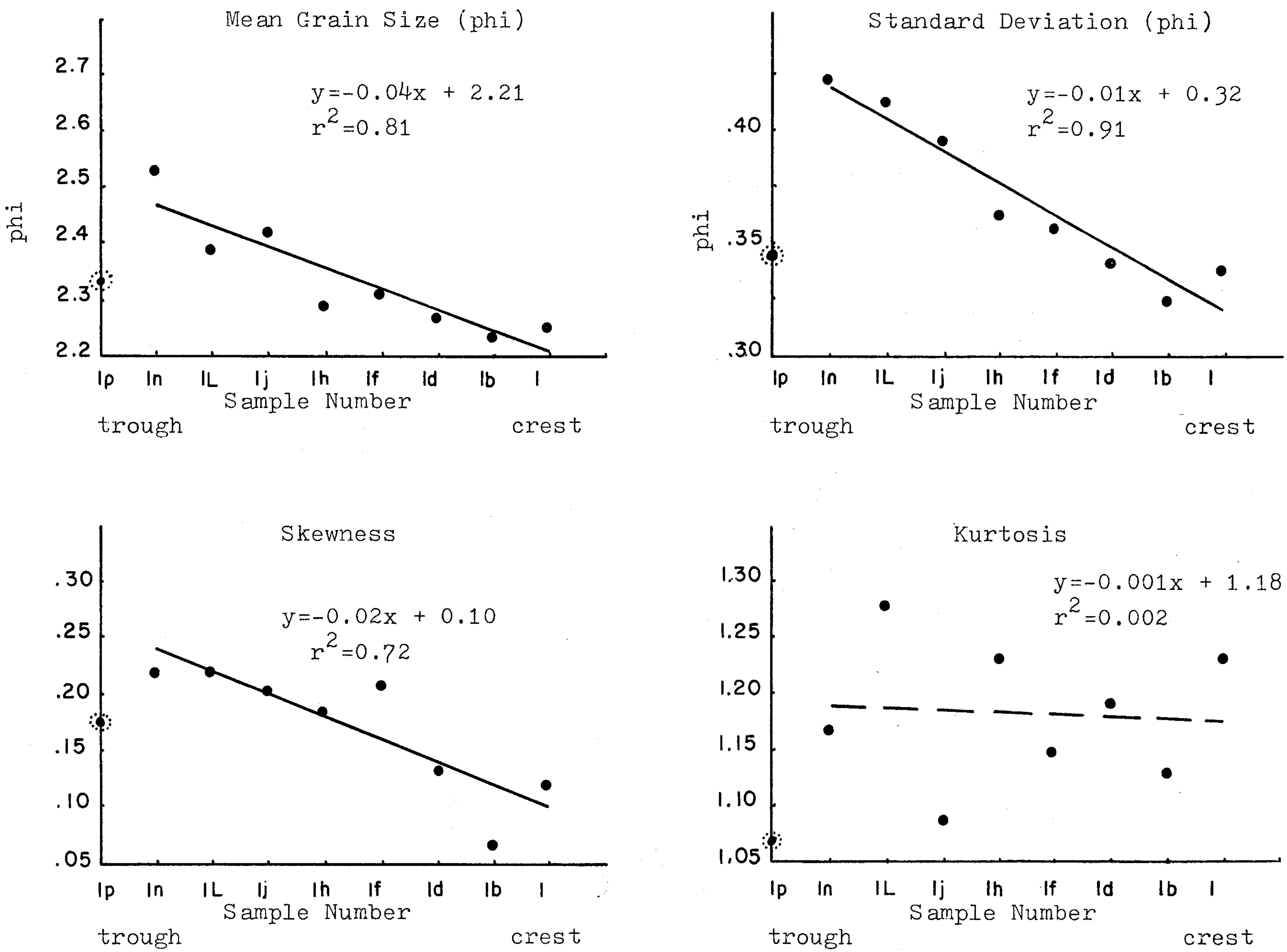
Mean Grain Size (phi)
y=-0.04x + 2.21
r2=0.81
phi
2.7
2.6
2.5
2.4
2.3
2.2
Ip In IL Ij Ih If Id Ib I
Sample Number
trough
crest
Standard Deviation (phi)
y=-0.01x + 0.32
r2=0.91
phi
.40
.35
.30
Ip In IL Ij Ih If Id Ib I
Sample Number
trough
crest
Skewness
y=-0.02x + 0.10
r2=0.72
.30
.25
.20
.15
.10
.05
Ip In IL Ij Ih If Id Ib I
Sample Number
trough
crest
Kurtosis
y=-0.001x + 1.18
r2=0.002
1.30
1.25
1.20
1.15
1.10
1.05
Ip In IL Ij Ih If Id Ib I
Sample Number
trough
crest

FIGURE 4.5: Variation in grain summary statistics on the slip face of sandwave ENB.

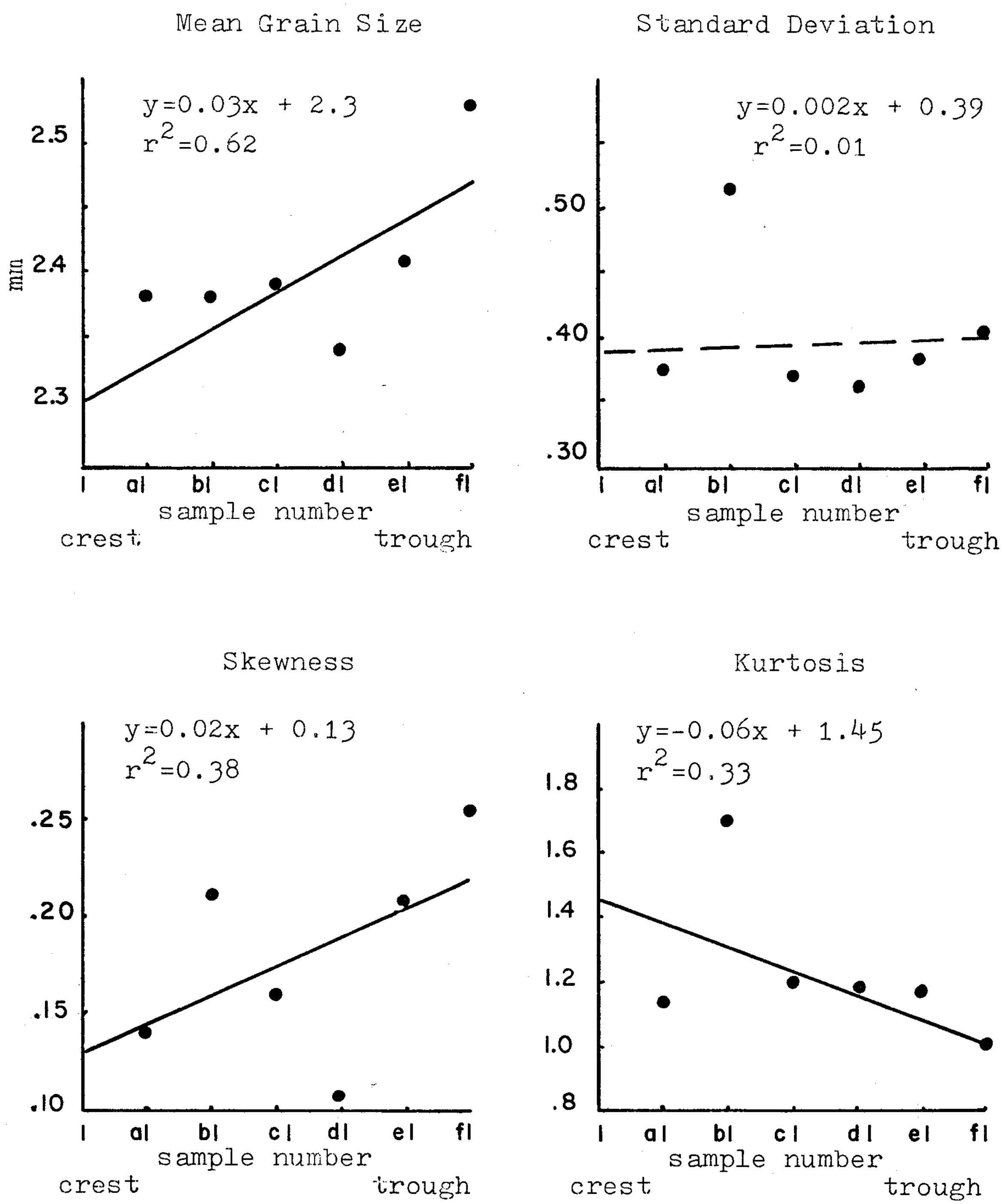

Mean Grain Size
y=0.03x + 2.3
r2=0.62
mm
2.5
2.4
2.3
I
a1
b1
c1
d1
e1
f1
sample number
crest
trough
Standard Deviation
y=0.002x + 0.39
r2=0.01
.50
.40
.30
I
a1
b1
c1
d1
e1
f1
sample number
crest
trough
Skewness
y=0.02x + 0.13
r2=0.38
.25
.20
.15
.10
I
a1
b1
c1
d1
e1
f1
sample number
crest
trough
Kurtosis
y=-0.06x + 1.45
r2=0.33
1.8
1.6
1.4
1.2
1.0
.8
I
a1
b1
c1
d1
e1
f1
sample number
crest
trough

would result in the winnowing of fines on the lower portion of the stoss side, leaving a coarser lag. The crest of the bedform is elevated above the general level of the bed, and is subjected to higher velocity currents, resulting in a higher average shear stress which is sufficient to transport even the coarsest grains. The coarsening trend down the slip-face has been observed by several authors (Allen, 1965, Basumallick 1966), and is thought to be the result of the avalanching which occurs periodically on the slipface.

The grain size variations on the rippled sand wave on East Noel Bar correspond to Dalrymple's (1977) type two pattern. The bedforms studied by Dalrymple which exhibited this pattern, did not have avalanche faces, while the ENB sandwave had a distinct slipface that was almost angle of repose. The identifying factor of this pattern is the concentration of coarse grains at the crest of the bedform. Figures 4.4a and 4.5a demonstrate the coarsening upward trend on both the stoss and slipfaces. Several explanations for this have been proposed by different authors (Jopling, 1965; Allen, 1968; Dalrymple, 1977), however a satisfactory explanation has not been published that could account for this pattern on both bedforms with and without avalanche faces.

It is possible that the magnitude of turbulence fluctuations could produce this type of grain size variation. McQuivey and Keefer (1969) have stated that "... over the crest of a ripple, where the relative intensity of turbulence is low, a particle is subjected to less shearing stress than it is in the trough where turbulence fluctuations are large." In other words, this means that the maximum shear stresses are found in the trough, even though the average shear stress is higher at the crest. This could result in the movement of coarser grains out of the trough and deposition of the grains at the crest where the turbulence variations are low and the shear stress would not be sufficient to initiate movement again. The finer grains could still be transported over the crest as traction load and would result in the formation of an avalanche face with finer grains at the base.

This appears to contradict the reasons put forth for the grain size pattern observed at SB-MIII. The current velocity of ENB is lower than at SB-MIII (average maximum flood and ebb velocity of about 0.8 m/sec compared to 1.0 m/sec; Knight, 1977), and the mean grain size is also smaller. It thus may be possible that at ENB the finer grain size is just small enough to allow the shear stress bursts, produced by the turbulence, to entrain the grains in the trough, while at SB-MIII the grains are too large to allow this to happen.

Chapter 5

V pits

A V-shape may be roughly defined as any triangular shaped indentation in the surface of a sand grain. V-shapes may be of two basic types: etch pits, or abrasion pits, and are produced by widely differing mechanisms.

Etch pits are often called chemical pits, solution pits or simply oriented V pits. These features are always found in groups with a single orientation that is controlled by the crystallographic axes in the quartz (Krinsley and Donahue, 1968). Etch pits are formed due to prefered solution at a defect in the crystal, and these defects may be caused by dislocations in the crystal structure, micro-fractures, impurities and even fission and alpha tracks (Amelinck, 1964 in Margolis, 1968). The size of etched pits can range from 50 micrometers to less than 1/10 micrometer (Krinsley and Doornkamp, 1973). Their outer edges are regular, and the inner surface is smooth and may be relatively flat (see figure 5.1a). When observed, these pits were not used for V pit density determinations, due to their solutional origin.

Middleton and Davis (1979) studied 1068 intertidal sand grains and stated that oriented V's produced by chemical solution are not present in Minas Basin intertidal sands.

FIGURE 5.1: Diagramatic sketch of V pit topography (adapted from Krinsley and Donahue, 1968)

Chemical V

1a

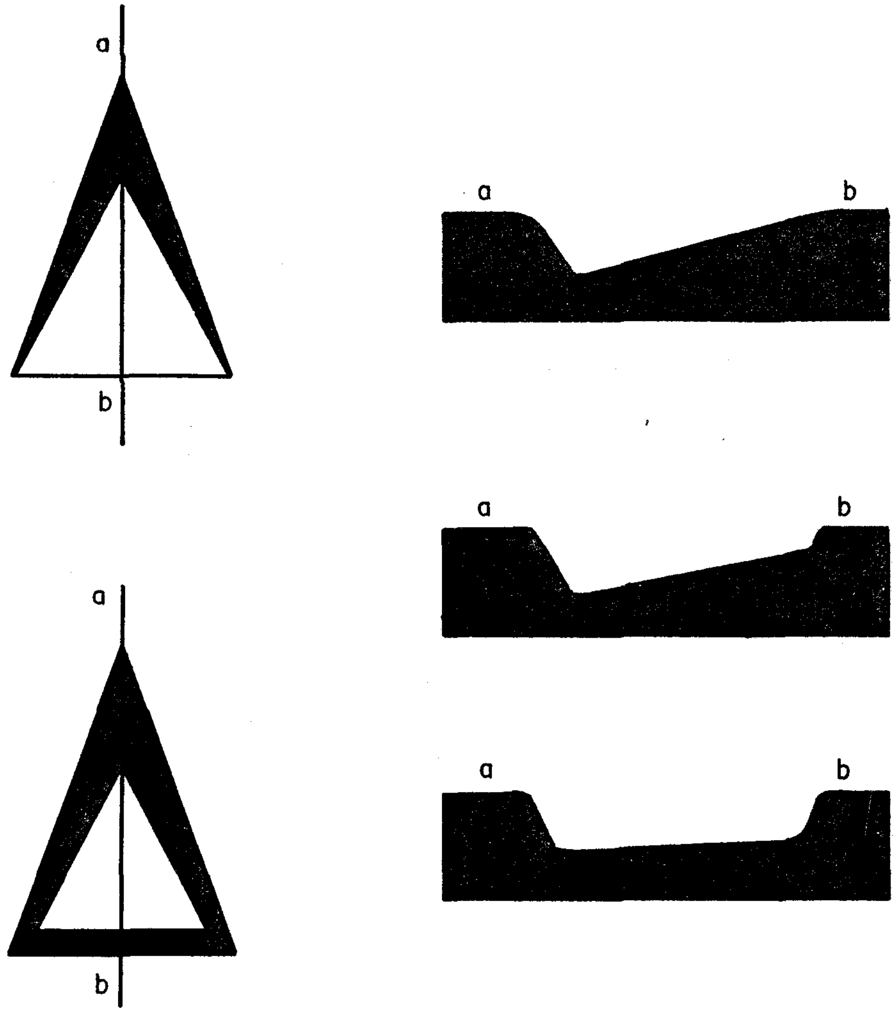

Mechanical V

1b

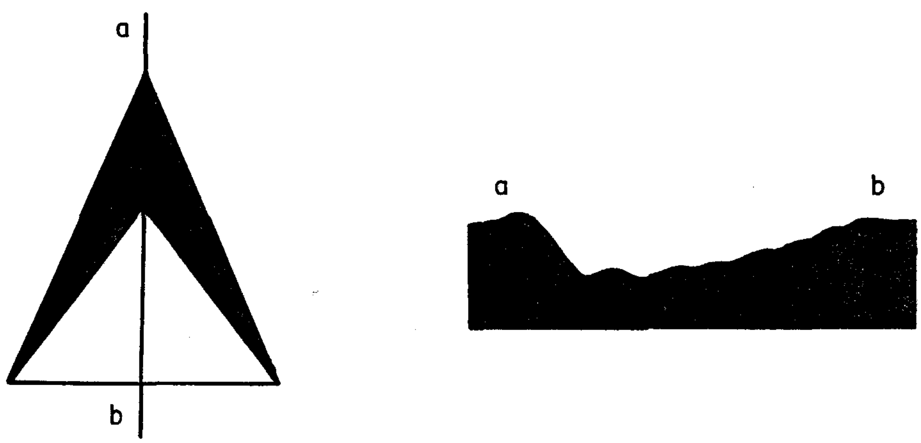

However, from a sample subsection of 112 intertidal sand grains observed in this study, at least 6 had areas with distinct etch pitting (see figure 5.2). The actual number of grains and the amount of chemical etching was not noted, as it was unimportant for this study. It therefore appears that chemical weathering is present in intertidal sands, but as noted in Middleton and Davis (1979), does not have a particularly strong effect.

Abrasion pits are also called mechanical V pits, impact pits or random V pits. They generally have a totally random distribution pattern, yet it has been noted in this study and by other investigators (Krinsley and Donahue 1968; Krinsley and Smalley, 1972), that partially oriented sets of impact pits do occur. A closely related feature is straight or lightly curved grooves with "satelite V's" (see figure 5.3), which are the result of high energy grain to grain impacts.

At high magnifications the large V pits do not show a regular smooth outline, and have a rough unevenly depressed center (figure 5.1b) formed by irregular chipping of parallel cleavage plates (Margolis and Krinsley, 1974). Grooves are formed only in moderate to high abrasion level environments, on grains larger than 400 to 500 micrometers in diameter, due to their greater impact force (Margolis and Krinsley, 1974). At low impact velocities the colliding grains may just slide across each other, rubbing off fine splinters of the surface, creating shallow, widely spaced V pits. At higher velocities,

FIGURE 5.2: Chemical etch pits

a- Magnification = 2500X

Scale bar equals ten micrometers

b- Magnification = 5000X

Scale bar equals one micrometer

a

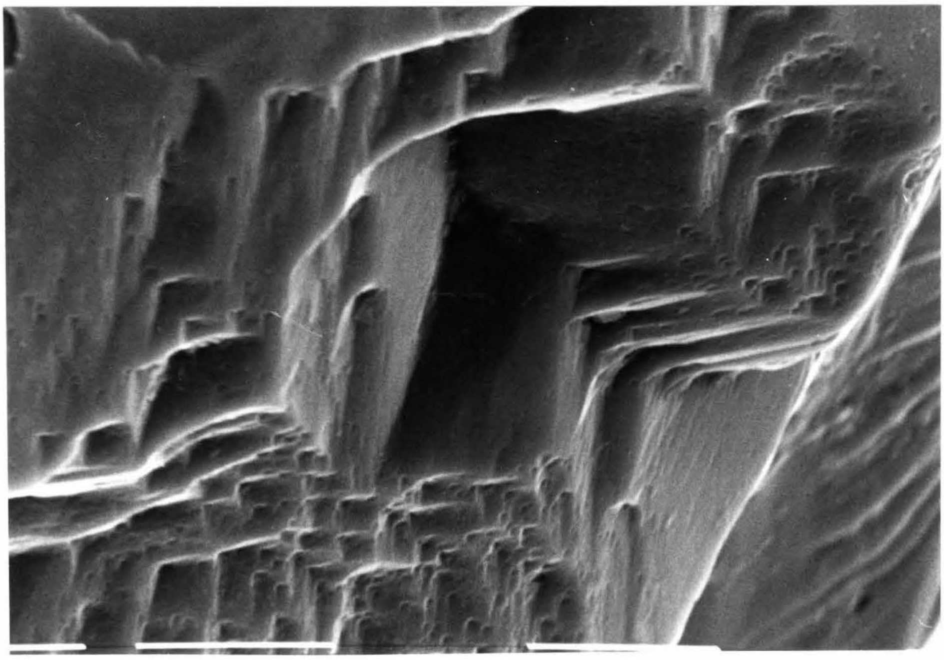

b

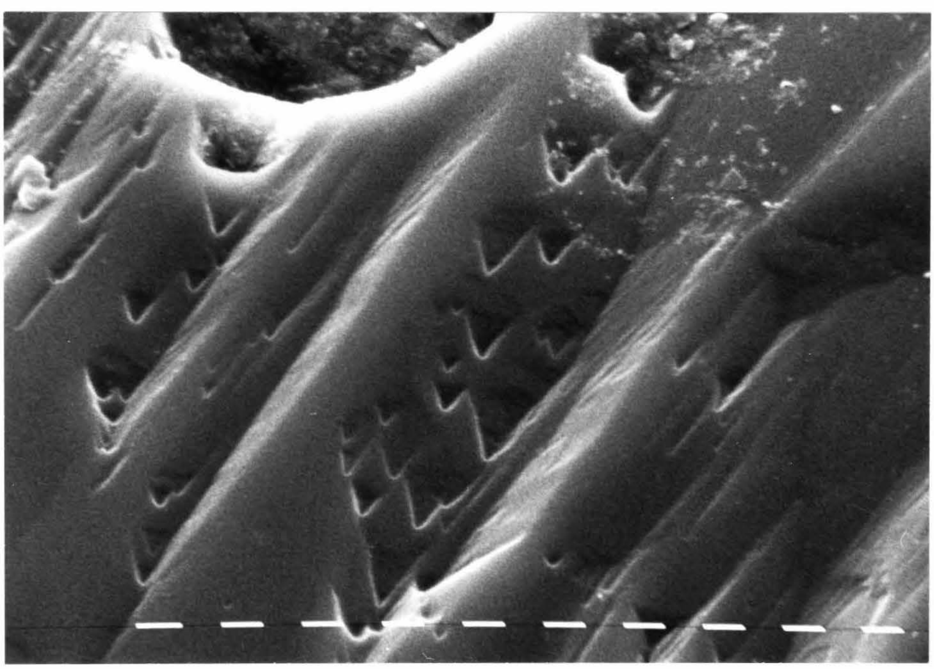

FIGURE 5.3: Curved grooves with "satellite V's"

a,b- Magnification = 10000X

Scale bar equals one micrometer

a

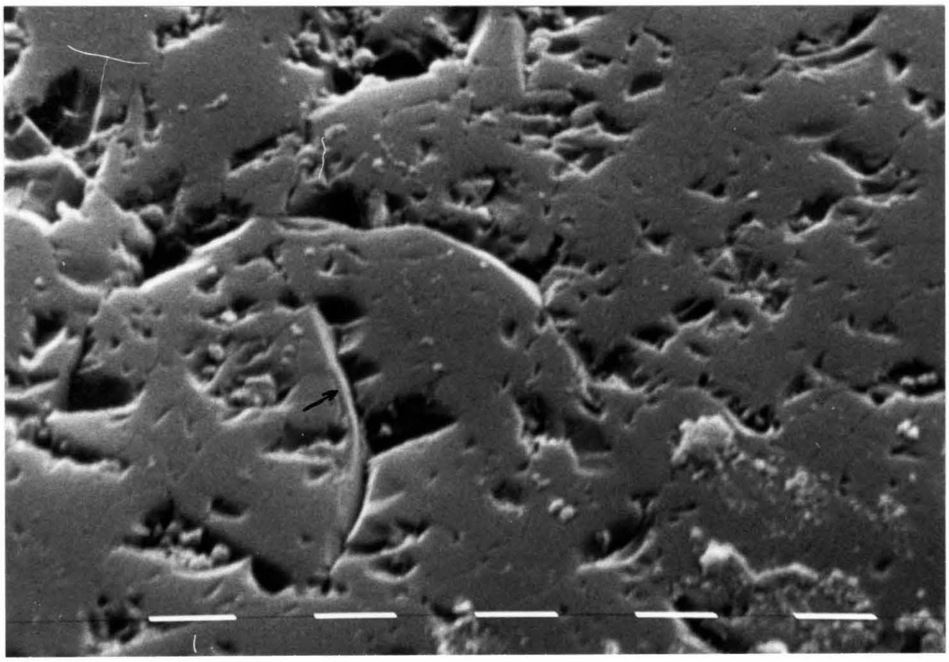

b

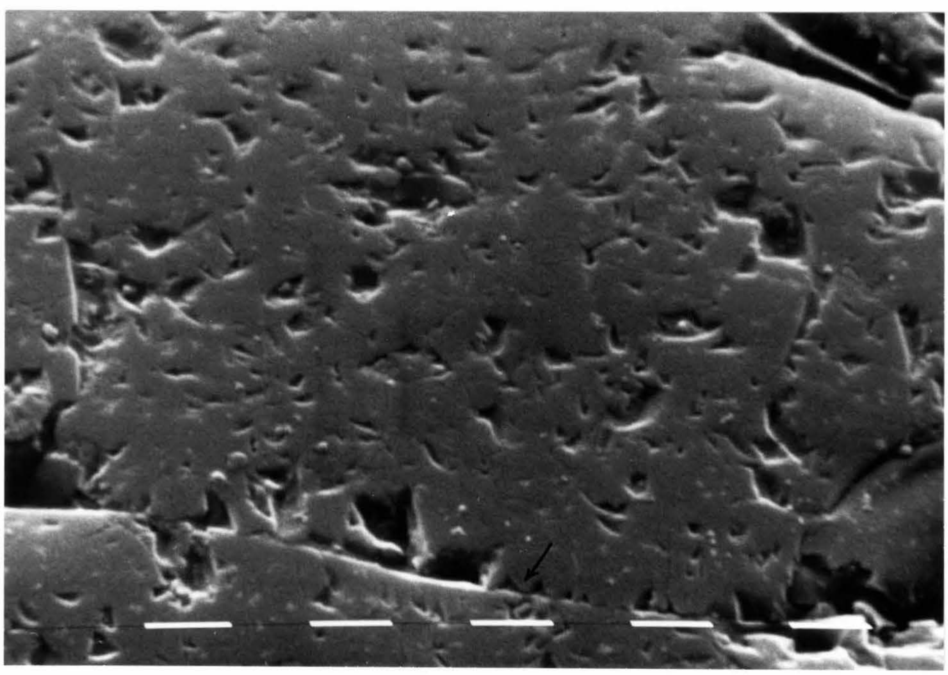

the V pits will be larger and deeper, with a higher density of pitting, and at some point the impacts will be strong enough to form grooves and V pits together at a single contact point (Margolis and Krinsley, 1974).

There are several problems that must be taken into account when studying V pits. V pits may be formed in several environments, and the density of pits is the result of the accumulation of impacts from all the environments the grain has been subjected to. Figure 5.4 lists these environments and indicates the relative amounts of impact features they produce.

Quartz grains are supplied from two major sources in the Minas Basin shoreline. The pleistocene deposits have grains with minor V pitting (Brisbin, 1974), and the Triassic sandstones which are primarily of fluvial and eolian origin (Hubert, 1980), also have V pits, but a relatively small amount, due to their origin (Davis, 1978). Thus most of the V pits identified on the intertidal sands should have occurred in the intertidal environment.

A further problem is time. Not all of the grains have spent the same amount of time in the intertidal environment, as new sediment is constantly being added from the eroding bluffs on the shoreline. Older grains would be expected to show a higher density of impact pits than fresh grains that have not had time to show the full effects of the new environment. It is impossible to distinguish new

FIGURE 5.4: Environmental occurrence of V pitting
(from Margolis and Krinsley, 1974)

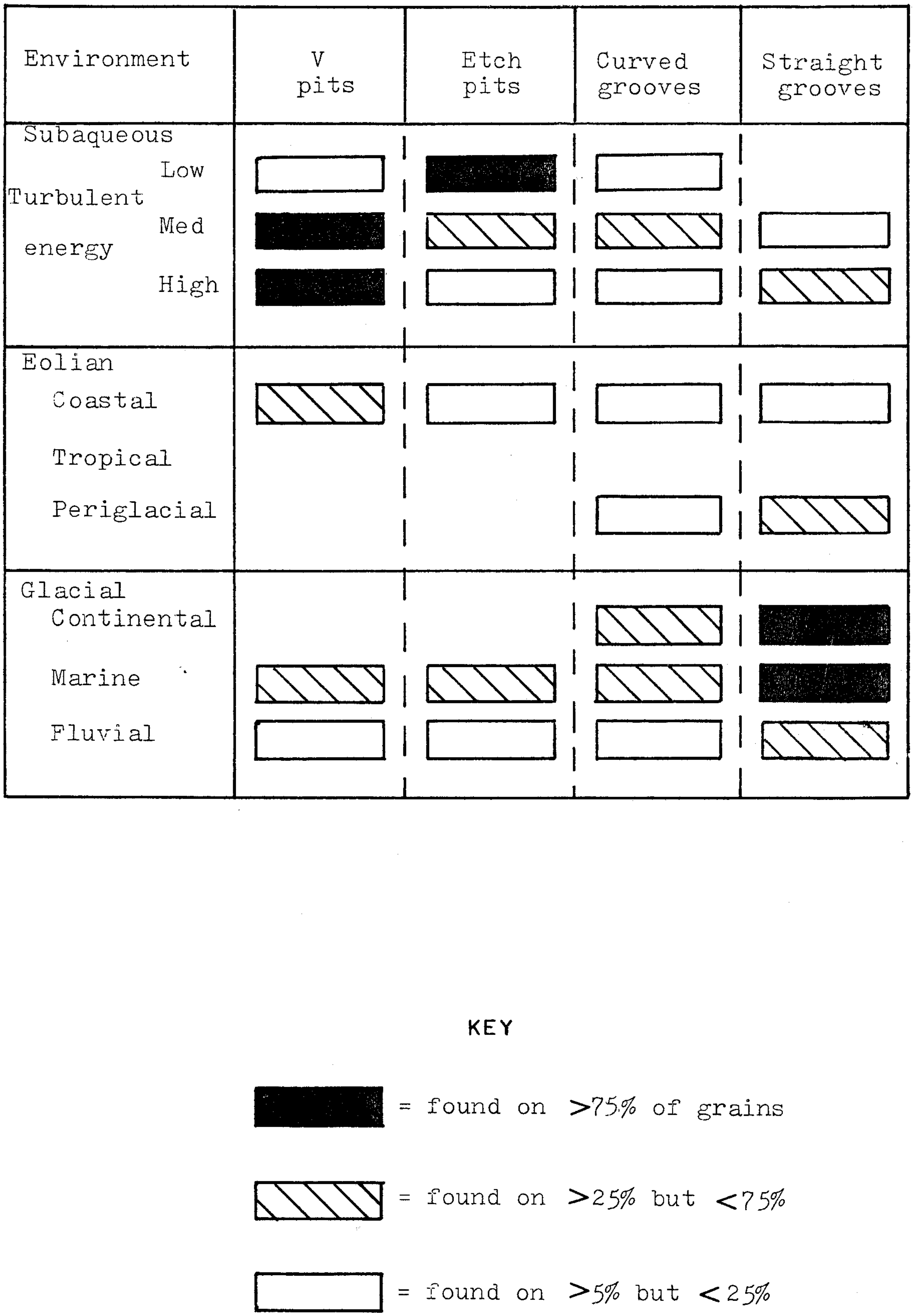

Environment
V pits
Etch pits
Curved grooves
Straight grooves
Subaqueous
Turbulent energy
Low
Med
High
Eolian
Coastal
Tropical
Periglacial
Glacial
Continental
Marine
Fluvial
KEY
= found on >75% of grains
= found on >25% but <75%
= found on >5% but <25%

grains from old ones by roundness, due to the variations in roundness from the sediment sources. This would be a partial cause for a large difference in V pit densities observed on grains of the same size. Another factor that is more important than time in the environment is the amount of time spent on the surface of the sand body, because this is what will determine the density of V pits.

A related problem is the deposition of silica on the surface of the sand grains. This occurs in intertidal and subtidal environments (Middleton and Davis, 1979; Hampton et al., 1978), and may form patchy growths or a smooth skin over a portion of the surface (see figure 5.5a). The result of this is to cover up and smooth out the old surface and to provide a fresh new unmarked surface (see figure 5.5b). The new surface would have a low V pit density, while other uncovered areas of the grain would show a much higher density if they were also observed.

This leads to the basic difficulty in quantifying V pit densities. The V pits occur on all exposed surfaces, but can only be recognised and counted with any degree of accuracy on smooth or polished areas. Rough areas with upturned cleavage plates do not allow the pits to stand out distinctly due to the jagged surface. Therefore the areas most likely to be used for density determination are smooth areas which may be original grain surfaces or may be areas of silica precipitation.

FIGURE 5.5: Silica precipitation

a- Magnification = 2500X

Scale bar equals ten micrometers

b- Magnification = 5000X

Scale bar equals one micrometer

a

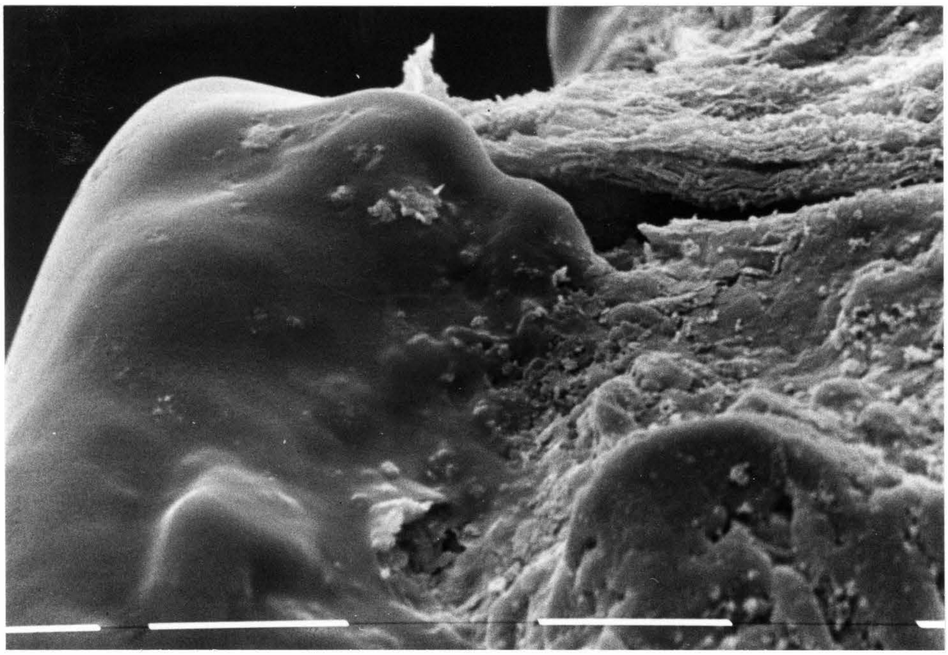

b

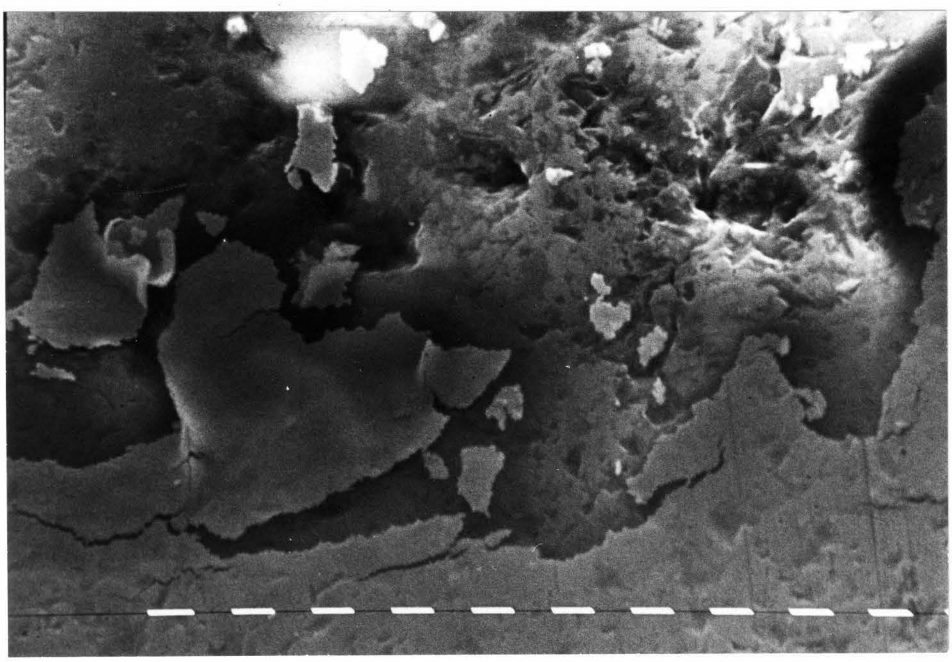

V pit density determination

Photographs were taken at magnifications of 5000 and 10000X using 35 mm B&W print film. The upper limit of 10000X was determined by the resolution of the SEM. Above this magnification, focussing was difficult and the time necessary to create a sharp image was too great. An electron beam spot size of 200Å could be used for both magnifications, allowing the operator to rapidly switch from one magnification to the other without major adjustments.

To keep the cost of the study down, the images were printed as proof sheets rather than individual prints. Nine prints, 7 x 9 cm in size were produced on a single sheet, allowing easier storage and handling. Due to the small size of the prints, the photographs taken at 5000X magnification were studied using a binocular microscope with a magnifying power of 8X. This allowed V pits of 1/5 micrometer or less in size to be identified. The overall poorer focus and the slightly blurred images in the photographs taken at 10000X magnification necessitated the use of a 3X magnifying desk lamp. This allowed identification of V pits down to at least 1/10 micrometer.

Initially it was hoped that an image analyser could be used to detect and count the V pits. It was soon realized that the shading differences between the V pits and the grain surface were not significantly different and could not be differentiated to a high enough degree of accuracy. Therefore the identification and counting was done by hand using the following method.

A clear sheet of plastic was placed over each photo and with the use of one of the magnifying devices, each V pit was marked with a dot. After this was completed another clear plastic overlay was placed on top. This sheet had two squares inscribed on it, one in the center of the other. On photos taken at 5000X magnification, the small central square had an area of 25 square micrometers while the outer one enclosed an area of 100 square micrometers, which included the inner square. This same sheet on the photos taken at 10000X magnification gave areas of 6.25 and 25 square micrometers respectively.

At the beginning of the work it had been arbitrarily decided to place the squares in the center of each photograph in order to remove any possibility of operator bias. The different magnifications and sample areas were used in order to observe their effect on the V pit densities obtained.

The number of V's inside each box were counted and the density of V pits per square micrometer were tabulated for the magnification and area sampled. Often several pictures were taken of different areas of the same grain, at the same magnification. These were then combined and an average V pit density for each of the grains was tabulated (see appendix 1).

Two samples were used for this portion of the study, samples SB-MIII and SB-I (For location see figure 2.1). Quartz grains ranging in size from +0.5 to +2.5 phi in half phi steps from sample SB-MIII, were used as a trial batch to become accustomed to V pit identification and counting. Quartz grains observed from sample SB-I ranged in size from -1.0 to +2.0 phi in half phi steps. These samples are from opposite sides of the sandbar, and were chosen to identify the effect of closeness to the shoreline, the source of new grains.

Klein (1970) suggested a "racetrack" type model in which sand circulated around the sandbars in a continuous circuit, one side of the bar being ebb dominated and one side flood dominated. This would suggest that the density of impact pits should be similar on both sides of the bar, assuming that the bar is a relatively long term equilibrium feature. It could be very possible that samples from SB-I, the southern side of the bar, would show a lower density of V pits due to the supply of fresh grains from the eroding shoreline and a maximum mean current speed for flood and ebb that is approximately 35% lower than the northern side of the bar (Knight, 1977).

The initial data indicated the exact opposite, that grains from sample SB-I had much higher V pit densities. However, when several of the photographs from sample SB-MIII were re-analysed, new V pit density values were obtained that were 30-40% higher than the original values. Due to time limitations, most of the photographs from sample SB-MIII could not be re-analysed. When the rough correction of 40% was applied, the samples from both sides of the sandbar had roughly similar V pit densities.

The values of V pit density obtained from grains from sample SB-MIII have not been included in this study due to their inaccuracies. Ten photographs of various grains from samples SB-I were also re-analysed, and the initial results were duplicated with better than 90% accuracy.

The reasons for the inaccurate and irreproducible results from sample SB-MIII are as follows. These grains were the first ones analysed, and it required a fair period of time before the operator was able to produce consistant, good quality photographs from the SEM. Experience is required to be able to rapidly select those areas of the grain where V pits would be abundant and easily countable. The major problem was in creating and maintaining a criterion for the identification of a V pit. Practice is the only answer, as a significant period of time is required to establish a consistant identification.

Results

Figure 5.6 indicates a linear correlation between V pit density and grain size, when measured in phi units. Linear regression by the method of least squares was used on data obtained from photos taken at 10000X using a sample

FIGURE 5.6: Mean V pit density versus grain size

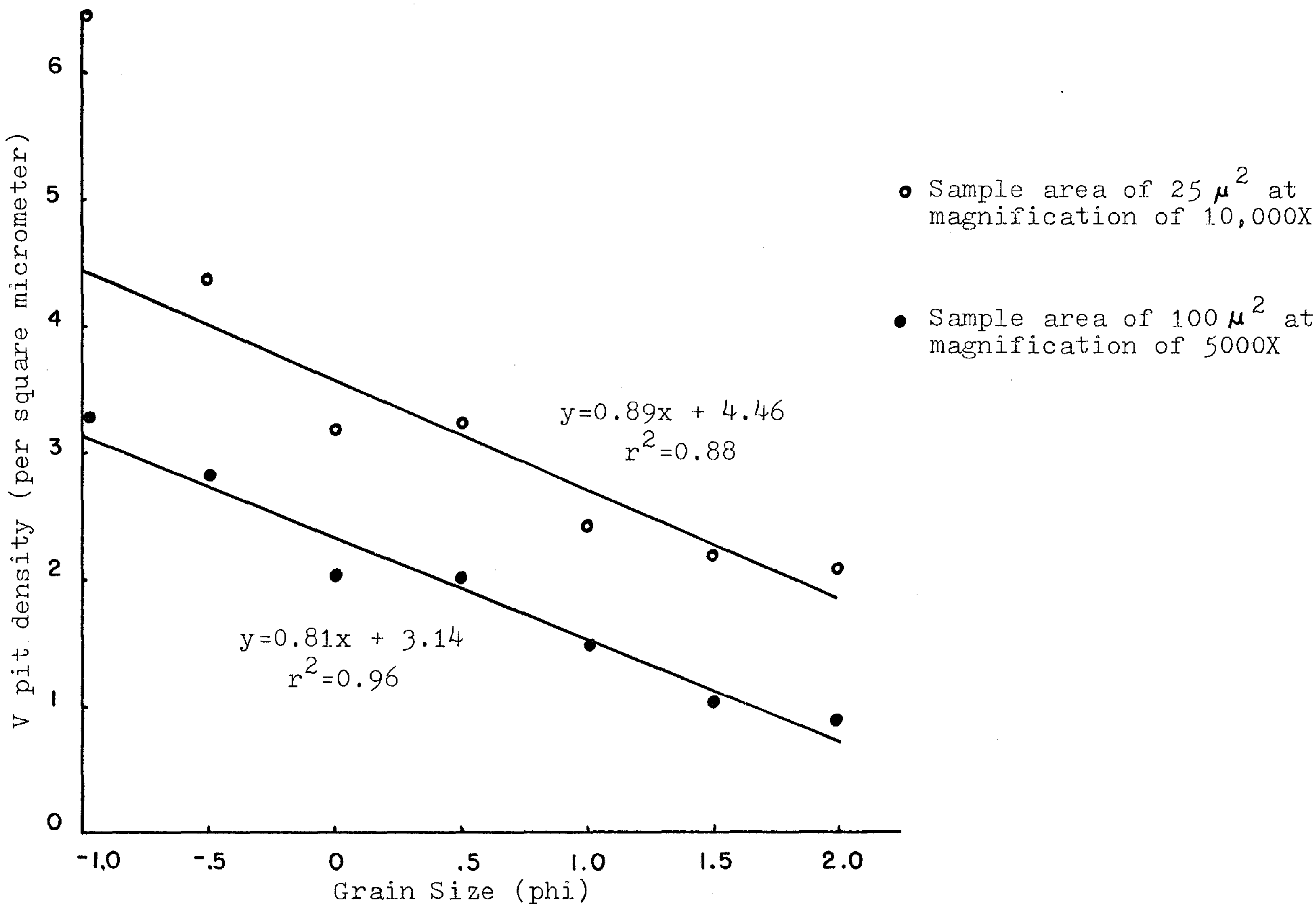

V pit density (per square micrometer)
0
1
2
3
4
5
6
-1.0
-.5
0
.5
1.0
1.5
2.0
Grain Size (phi)
y=0.89x + 4.46
r2=0.88
y=0.81x + 3.14
r2=0.96
Sample area of 25 μ2 at magnification of 10,000X
Sample area of 100 μ2 at magnification of 5000X

area of 25 square micrometers and photos taken at 5000X using a sample area of 100 square micrometers. These data groups were chosen because they represent the largest sample areas used for each magnification, and these two formats had overall low standard deviations, suggesting more accurate and consistent results (see table 1).

Only one data point was excluded due to an anomalously high value. This point was calculated from only one photograph of a single grain and cannot be considered reliable. The slopes of both regression lines are very similar, and the coefficients of determination, r^2, indicate a good fit to the data. The similar slopes indicate a constant difference between the corresponding V pit densities obtained from the two different magnifications. This suggests that the number of small V's that are only visible in photos taken at a magnification of 10000X remain constant for all the grain sizes studied. This is rather unexpected, as the small grains carried in intermittent suspension should collide with less force and therefore produce smaller V pits.

The linear relationship shown in figure 5.6 is related to grain size that is measured in phi units. The phi scale was defined as $\phi = -\log_2 d$ by Krumbein in 1934. The same values for the density of V pits are plotted against grain size as measured in millimeters in figure 5.7 in order to emphasize the grain size changes.

TABLE 5.1: V pit density summary statistics

(Duplications - means the number of times a single location on the grain was photographed at both magnifications)

Magnification	10000X		5000X	
Area Sampled	6.25 μ^2	25 μ^2	25 μ^2	100 μ^2
Grain Size (phi)	-1.0			
Mean "V" density	5.44	6.40	4.52	3.27
Standard deviation	-	-	-	-
No. grains analysed	1	1	1	1
No. pictures analysed	1	1	1	1
Duplications	1			
Grain Size (phi)	-0.5			
Mean "V" density	5.00	4.38	3.62	2.84
Standard deviaition	0.97	0.74	0.48	0.22
No. grains analysed	3	3	2	2
No. pictures analysed	6	6	2	2
Duplications	1			
Grain Size (phi)	0.0			
Mean "V" density	3.59	3.20	1.99	2.00
Standard deviation	1.10	0.66	0.26	0.25
No. grains analysed	8	8	3	3
No. pictures analysed	16	16	4	4
Duplications	2			
Grain Size (phi)	+0.5			
Mean "V" density	3.38	3.26	2.21	1.99
Standard deviation	0.63	0.42	0.36	0.40
No. grains analysed	12	12	12	12
No. pictures analysed	21	21	18	18
Duplications	10			

Magnification	10000X		5000X	
Area Sampled	6.25 μ^2	25 μ^2	25 μ^2	100 μ^2
Grain Size (phi)	+1.0			
Mean "V" density	2.49	2.40	1.57	1.41
Standard deviation	0.54	0.55	0.47	0.22
No. grains analysed	11	11	9	9
No. pictures analysed	19	19	16	16
Duplications	8			
Grain Size (phi)	+1.5			
Mean "V" density	2.32	2.15	1.11	1.00
Standard deviation	0.57	0.56	0.32	0.23
No. grains analysed	8	8	9	9
No. pictures analysed	11	11	19	19
Duplications	5			
Grain Size (phi)	+2.0			
Mean "V" density	2.47	2.08	0.96	0.90
Standard deviation	1.37	1.12	0.44	0.39
No. grains analysed	9	9	7	7
No. pictures analysed	11	11	12	12
Duplications	5			

FIGURE 5.7: Mode of transportation break point in V pit density versus grain size.

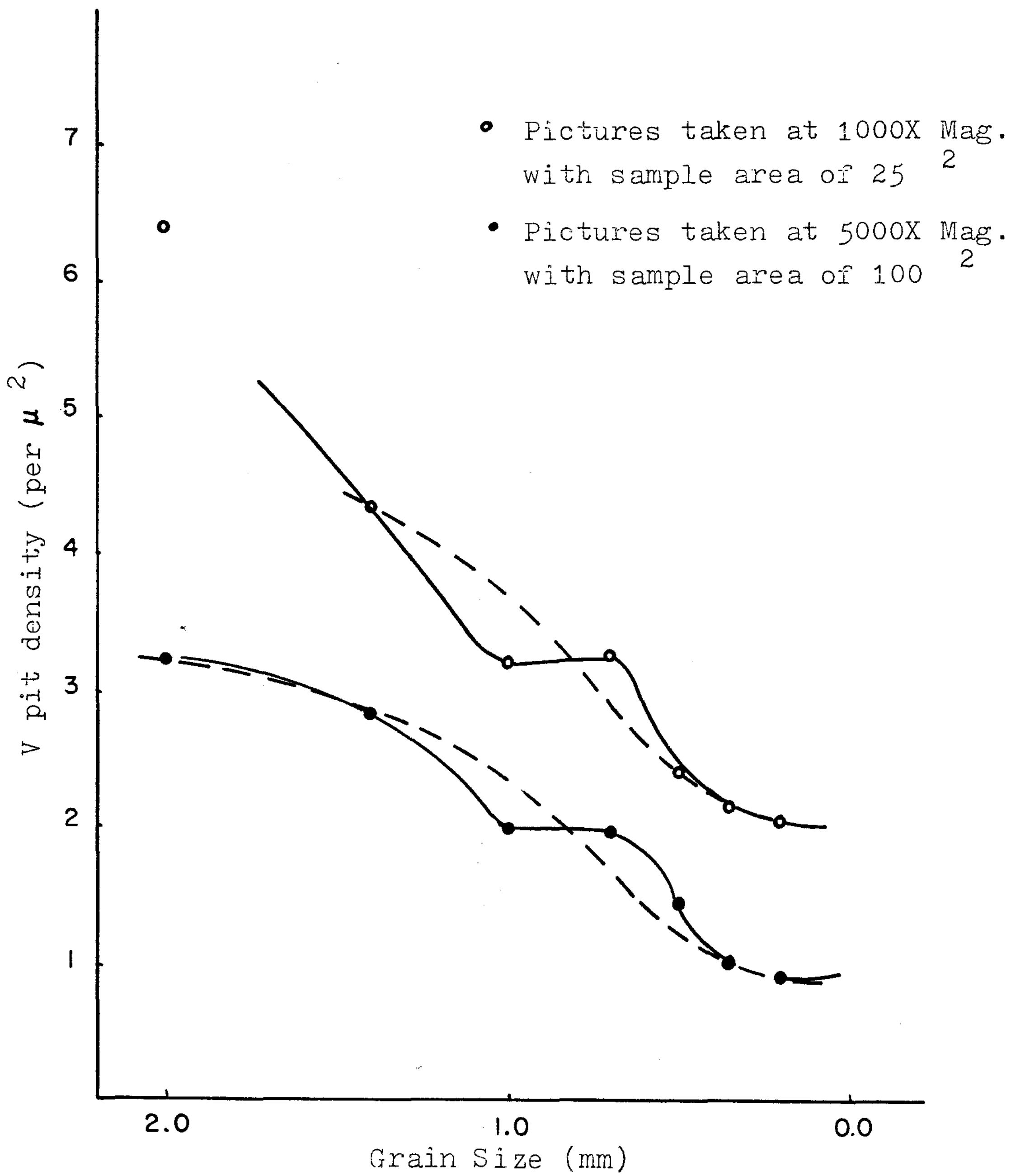
Pictures taken at 1000X Mag.
with sample area of 25 2
Pictures taken at 5000X Mag.
with sample area of 100 2
V pit density (per μ 2)
7
6
5
4
3
2
1
2.0
1.0
0.0
Grain Size (mm)

A smooth curve joining all the data points shows a plateau (which can also be seen in figure 5.6) for both magnifications at grain sizes between 1.0 and 0.71 mm. Figure 5.7 also shows a smooth curve drawn by eye as a best fit line for the data points. The inflection point occurs at a grain size of 0.81 mm, near the center of the plateau. A value of 0.81 mm is equivalent to a grain size of 0.2 phi, which is very close to the 0.5 phi value calculated as the "break-point" between traction and intermittent suspension populations by Middleton and Davis (1979), from several samples from the south side of Selmah bar. This size of 0.5 phi also corresponds to the upper size limit of grain suspension as calculated from current velocities by Dalrymple (1977) from the south side of Selmah Bar.

As shown in table 1, the V pit densities obtained from -1.0 and -0.5 phi size grains are the result of only a few photographs and cannot be taken as accurate values. Table 1 also indicates the number of times a single location on a grain was photographed at both 5000 and 10000X magnifications. This is very important as it could be the reason that the 5000X and the 10000X magnification photos produce results which are so similar. A maximum of 55%, and an average of 40% of the photographs were taken at both magnifications at the same site. This is not sufficient to account for the similarities noted in figures 5.6 and 5.7. Thus both sets of data provide independent corroboration of this break point.

The break point as defined by V pit densities should correspond to the values obtained by graphical analysis and actual shear velocity readings obtained from the general sample region. The traction population, (C), will spend most of its time on or near the bed, and thus will have collisions more often, due to the greater number of grains in motion there. The intermittent suspension population, (A), will spend varying amounts of time moving up in the water column. The amount of time a grain will spend in suspension, and the height that it will be lifted above the bed will be a function of its size. This results in the rapid slope changes in figure 5.7, which appear to approach an asymptote as grain size approaches zero.

The plateaus of V pit density observed at 1.0 to 0.71 mm (1.0 to 0.5 phi) in figure 5.7 appear to indicate that two different sizes of grains are acting in a manner which produces similar V pit densities. It is possible that two different factors are controlling the formation of V pits; one operates for large grains moved by traction, and the other for smaller grains moved in intermittent suspension (Middleton, pers. comm.). Figure 5.8 indicates both trends and the resultant V pit density produced by the combination of both trends.

Trend 1 operates on larger grains moved by traction, which are bombarded by saltating or intermittently suspended

FIGURE 5.8: Diagramatic sketch of two modes of V pit formation

(from Middleton, pers. comm.)

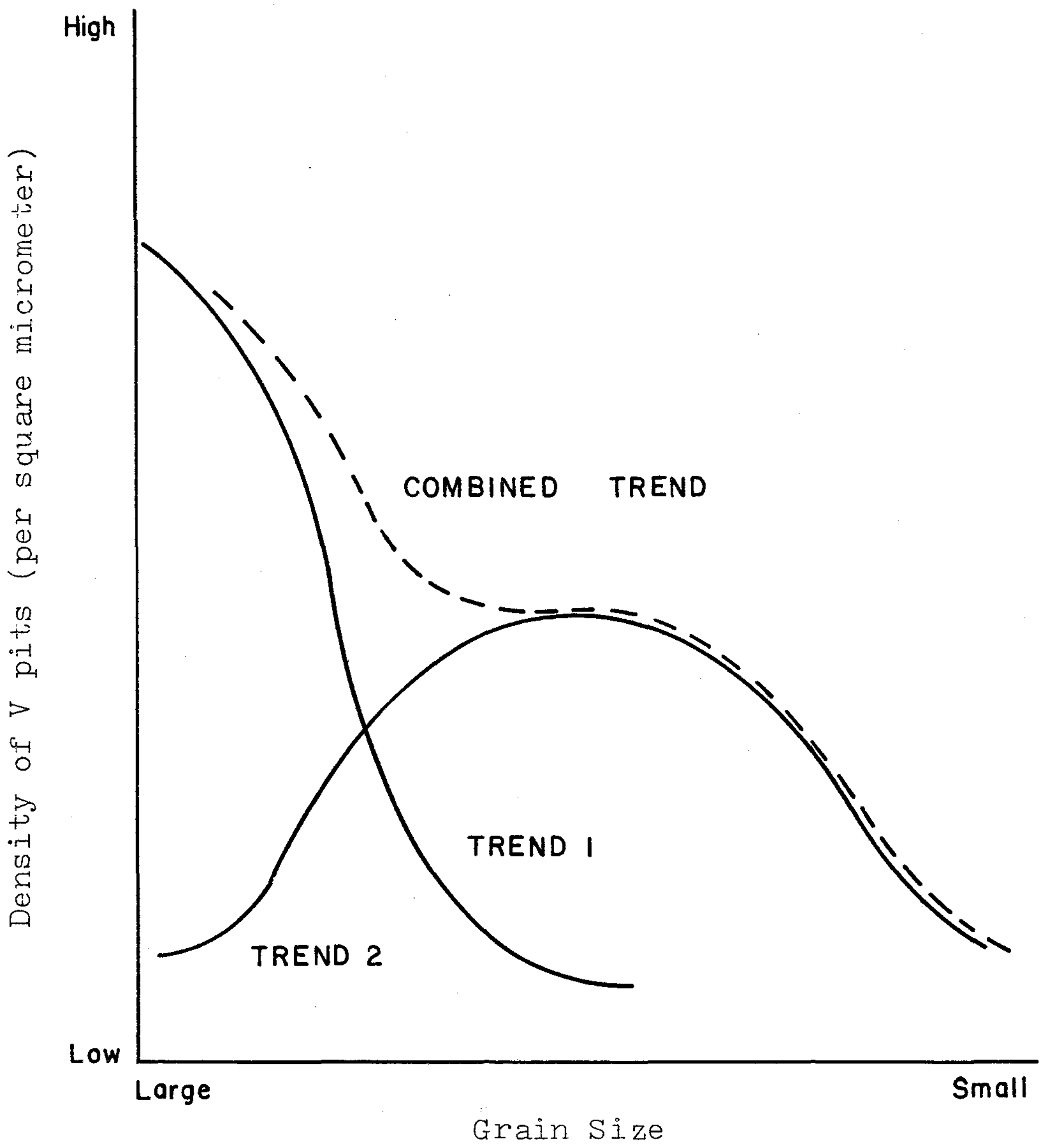
High
Low
Density of V pits (per square micrometer)
COMBINED TREND
TREND 1
TREND 2
Large
Small
Grain Size

grains. The grain must be sufficiently larger than the surrounding grains on the bed in order to be exposed to collisions. As its size decreases and approaches the mean grain size, the grain is less well exposed and fewer collisons result.

Trend 2 operates on grains in intermittent suspension in the concentrated "rheological layer" (Moss, 1972, in Middleton and Southard, 1977) close to the bed. Collisions are abundant in this layer due to the large number of grains in motion. Larger grains are not abundant in this layer because they cannot be suspended easily, and thus undergo fewer collisions. However, these grains are still not large enough to be well exposed on the bed, as the yet larger grains in the traction layer. As the grain size decreases past a critical size, the grains become too easily suspended and don't spend much time in the rheological layer, resulting again in fewer collisions.

Figure 5.9 illustrates the effect of varying the area of the grain surface sampled for both 5000 and 10000X magnification. The results do not differ too greatly, aside from the coarser grain sizes where the number of grains sampled was small. For both magnifications the smaller sampling area yielded higher V pit densities. This is due to the methodology used in this study. When taking pictures of the grain surface with the SEM, the operator, by arbitrary choice at the initiation of this study, always placed the

FIGURE 5.9: Variations in V pit density due to changes in sampling area.

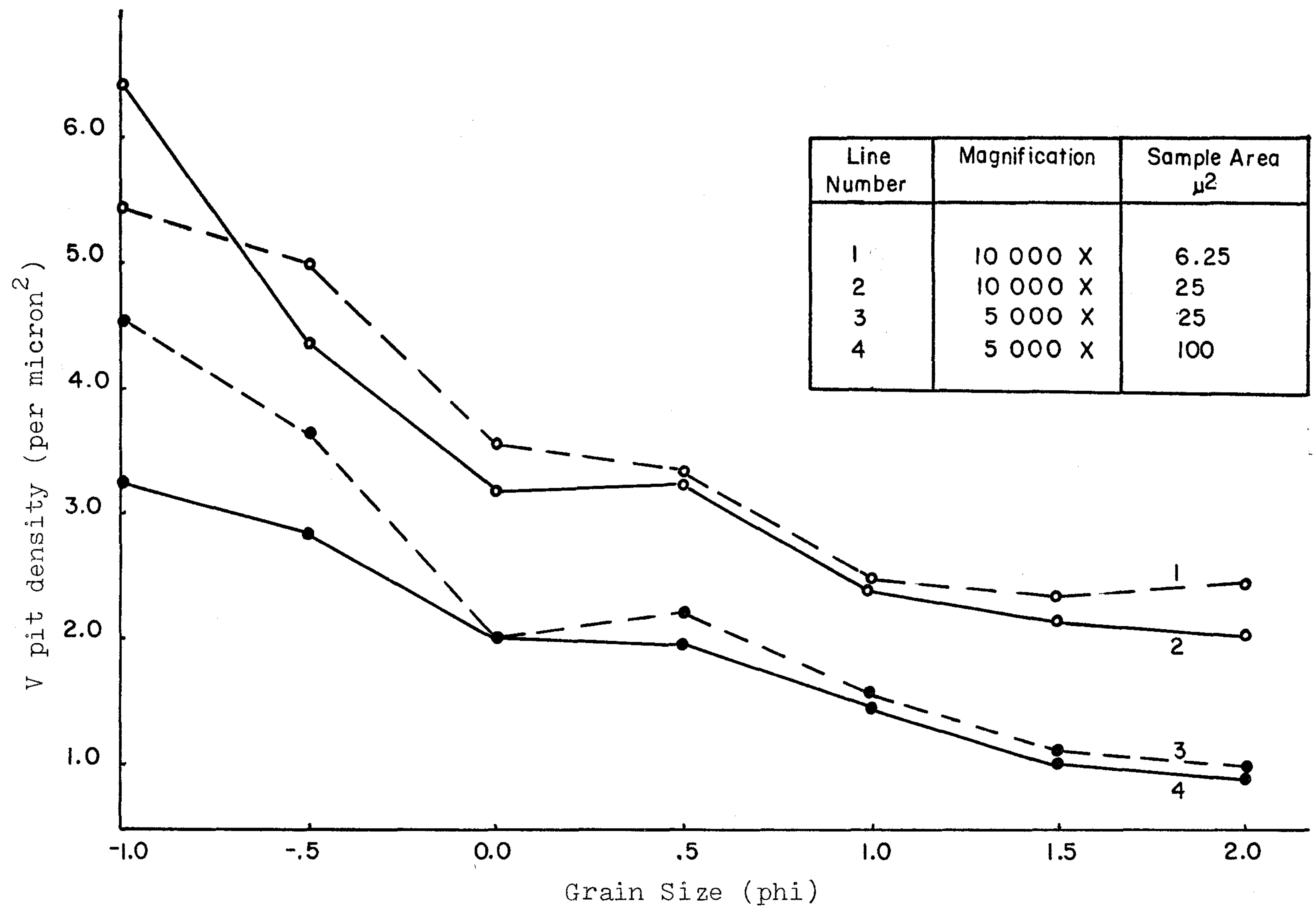
6.0
5.0
4.0
3.0
2.0
1.0
V pit density (per micron^2)
-1.0
-.5
0.0
.5
1.0
1.5
2.0
Grain Size (phi)
1
2
3
4
Line Number
Magnification
Sample Area μ^2
1 10 000 X 6.25
2 10 000 X 25
3 5 000 X 25
4 5 000 X 100

best area in the center of the photograph. The smaller, central square of the clear plastic overlay was always placed in the center of each photograph, and therefore produced higher values.

In most cases, two photographs of different locations were analysed to represent the V pit density of that grain. In some cases only one photo was usable, and the values obtained from it were used as representative of the whole grain. As a rough check of the validity of this method, one grain was photographed at 5000X magnification at six different locations. The mean V pit density was 0.85 pits per square micrometer, with a standard deviation of 0.17. This is equivalent to 20% of the mean V pit density and signifies a substantial variation. It therefore is not really valid to identify the mean V pit density of a grain from two areas on its surface, however time limitations did not allow a more extensive study. The values obtained were assumed to be representative for the whole grain even though this is not truly accurate.

Grain roundness was estimated using a Powers' (1953) visual comparison chart (AAPG, Memoir 28). No relationship was discovered between V pit density and grain roundness, as illustrated in figure 5.10. This is surprising in view of Balazs and Kleins' (1972) conclusion that quartz sand grains undergo considerable rounding in the intertidal environment. If this were true, then the more rounded grains

FIGURE 5.10: Effect of grain roundness on V pit density

Grain Roundness: VA = very angular
A = angular
SA = subangular
SR = subrounded
R = rounded
WR = well rounded

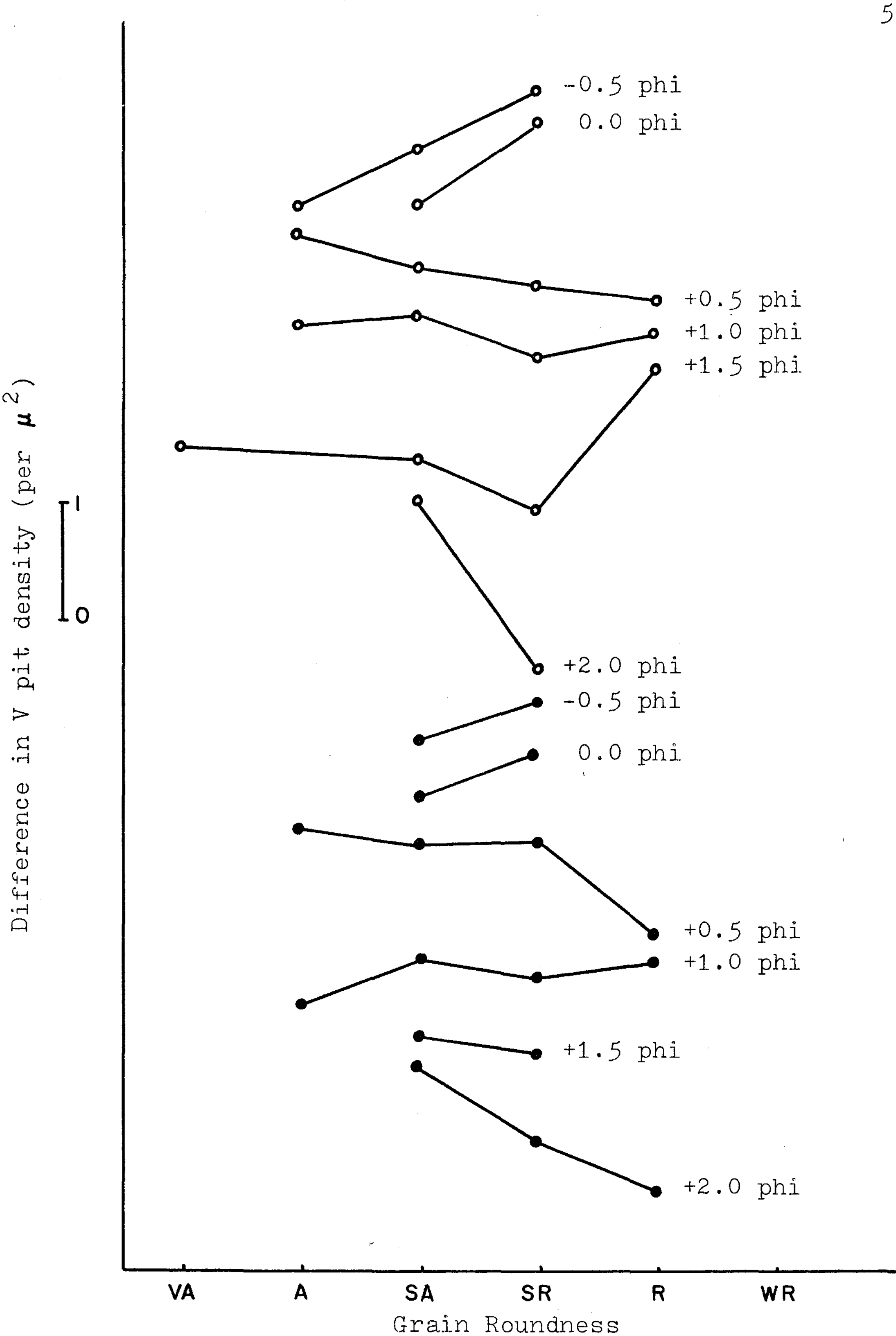
-0.5 phi
0.0 phi
+0.5 phi
+1.0 phi
+1.5 phi
+2.0 phi
-0.5 phi
0.0 phi
+0.5 phi
+1.0 phi
+1.5 phi
+2.0 phi
1
0
Difference in V pit density (per μ^2)
VA
A
SA
SR
R
WR
Grain Roundness

should show distinctly higher densities of V pits, since much of the rounding should be due to abrasion. Middleton and Davis (1979) noted that the percentage of grains showing impact pits varies with roundness. Less than 20% of angular grains showed V pitting, and up to 80% of the rounded and well rounded grains were pitted. This variation was not noted in this study. Angular grains do have less surface area available for impacting due to numerous low, protected areas.

Middleton and Davis (1979) conclude that much of the grain roundness observed in the intertidal sands is derived from the Triassic rocks forming the shoreline bluffs. This conclusion may also be drawn from figure 5.10, which indicates that rounding due to abrasion is not a major or rapid process in intertidal sands.

Many authors (Krinsley _et_ _al_., 1964; Krinsley _et_ _al_., 1973; Middleton and Davis, 1979) have noted that there are no major differences in the types of textures found on grains of different sizes. Very few studies have been published on the differences in the frequency of a texture on various grain sizes, or the frequency in different environments. Margolis and Kennett (1971) published a diagram, (see figure 5.11), which relates the density of impact pits with the amount of grains with impact pits on more than 10% of the surface. They do not indicate the grain sizes or the magnifications used to obtain the data.

FIGURE 5.11: Evolution of impact pits on quartz grains from subaqueous environments (after Margolis and Kennett, 1971)

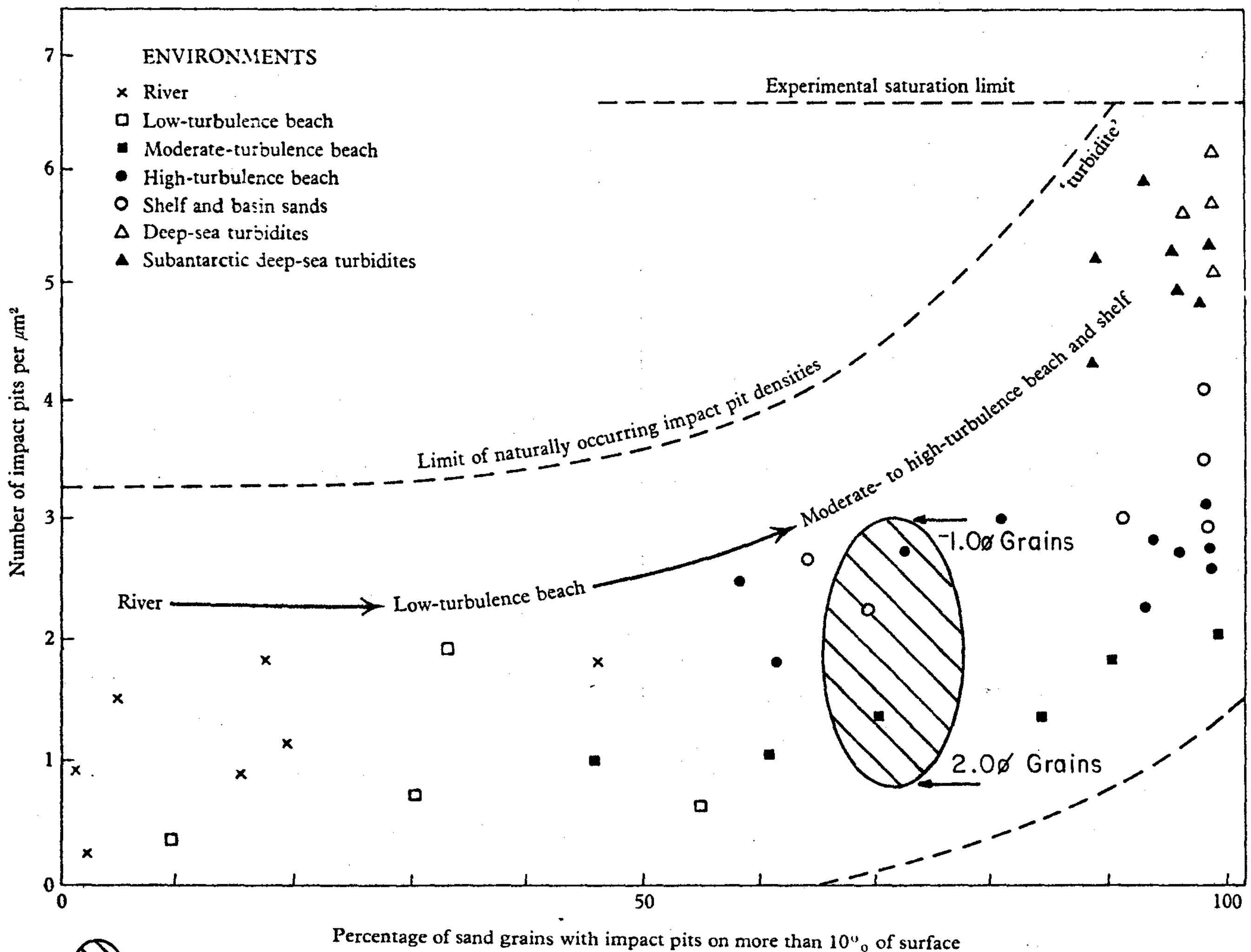


data from sample SB-I using a magnification of 5000X and a sample area of 100 μ^2

Data from this study has been plotted on this, and falls in the region labelled moderate to high turbulence beach and shelf sands. This is realistic considering that the tidal currents reach velocities in the order of 1 m per second. If data from this study obtained from photos taken at 10000X magnification were to be plotted on this diagram, it would lie at what Margolis and Kennett(1971) have defined as the upper limit of naturally occurring pit densities.

Chapter 6

Conclusions

1) The grain size distribution patterns over the two bedforms agree with Dalrymples' (1977) findings. The type one pattern is characterized by fining toward the crest, while the type two pattern coarsens toward the crest. The reasons for these two patterns are not well understood and further research is necessary in order to explain the differences.
2) Chemical solution of quartz grains and the formation of etched V pits does occur in Minas Basin intertidal sands. It does not have a strong effect and is greatly overwhelmed by mechanical activity.
3) There is a linear correlation between V pit density and grain size, with higher densities for larger grains.
4) The number of small V's (less than approximately 1/5 micrometer) does not vary with grain size, with the result that densities measured at higher magnifications closely follow values obtained at lower magnifications.
5) It is possible to arrive at a close estimate of the break point in grain size between the traction population (C), and intermittent suspension population, (B), from measurements of V pit densities.
6) There appears to be two trends producing V pits, with the

result that several different grain sizes have similar V pit densities. Bombardment of large, well exposed grains (transported in the traction layer) by smaller saltating grains, as well as grain impacts between smaller grains in the concentrated rheological layer result in a combined trend with a well defined plateau at a grain size corresponding to the initiation of intermittent suspension.

7) The density of V pits and the amount of occurrence on quartz grains can be used to classify the energy (turbulence) of the environment.

8) There is no correlation between grain roundness and V pit density, indications that the grains are not substantially rounded in the intertidal environment.

REFERENCES

Allen, J.R.L., 1965

Allen, J.R.L., 1968, The Diffusion of Grains in the Lee of Ripples, Dunes and Sand Deltas, J. Sed. Pet., V.38, No. 2, p. 621-633.

Amos, C.L., and Long, B.F.N., 1980, The Sedimentary Character of the Minas Basin, Bay of Fundy, Geol. Sur. Can., Paper 80-10, p. 153.

Baker, H.W., 1976, Environmental Sensitivity of Submicroscopic Surface Textures on Quartz Sand Grains - a Statistical Evaluation, J. Sed. Pet., V. 4, p. 871-880.

Balazs, R.J., and Klein, G. deV., 1972, Roundness - Mineralogical Relations to Some Intertidal Sands, J. Sed. Pet., V. 42, No. 2, p. 425-433.

Basumallick, S., 1966, Size Differentiation in a Cross-Stratified Unit, Sedimentology, V. 6, p. 35-68.

Blackwelder, P.L., and Pilkey, O.H., 1972, Electron Microscopy of Quartz Grain Surface Textures: The U.S. Eastern Atlantic Continental margin, J. Sed. Pet., V. 42, No. 3, p. 520-526.

Brisbin, D., 1974, A Comparison of Pleistocene Source Material Sands and Intertidal Sands, Minas Basin, Bay of Fundy, Unpublished Tech. Memo 74-5, McMaster University, August, 1974.

Brown, J.E., 1973, Depositional Histories of Sand Grains From Surface Textures, Nature, V. 242, p. 396-398.

Dalrymple, R.W. (1977), Sediment Dynamics of Macrotidal Sand Bars, Bay of Fundy. Unpublished Ph.D. Thesis, McMaster University.

Davis, P.M., 1978, Analysis of Microtextures on Quartz Sand Grains of Triassic Age, From the Minas Basin-Cobequid Bay Area, Nova Scotia. Unpublished B.A. Thesis, McMaster University.

Dickson, M., 1974, The Sieve Method of Size Analysis; An Instructional Manual. Unpublished Tech. Memo 74-3, McMaster University.

Folk, R.L., 1980, Petrology of Sedimentary Rocks, Hemphill Publishing Co., Austin Texas.

Grant, D.R., 1970, Recent Coastal Submergence of the Maritime Provinces, Canada, Can. Jour. Earth Sci., V. 7, p. 676-689.

Hampton, M.A., Bouma, A.H., and Torresan, M.E., and Colburn, I.P., 1978, Analysis of Microtextures on Quartz Sand Grains from Lower Cook Inlet, Alaska, Geol., V. 6, p. 105-110.

Hubert, F.J., and Mertz, K.A., 1980, Eolian Dune Field of Late Triassic Age, Fundy Basin, Nova Scotia, Geology, V. 8, p. 516-519.

Ingersoll, R.V., 1974, Surface Textures of First Cycle Quartz Sand Grains, J. Sed. Pet., V. 44, No. 1, p. 151-157.

Jopling, A.V., 1965, Laboratory Study of the Distribution of

Grain Sizes in Cross-Bedded Deposits, In Primary Sedimentary Structures and their Hydrodynamic Interpretation (ed. G.V. Middleton). Soc. Econ. Paleont. and Mineral., Spec. Pub. No. 12, p. 53-65.

Jopling, A.V., 1966, Origin of Laminae Deposited by the Movement of Ripples along a Streambed: a Laboratory Study, Jour. Geol., V. 75, p. 287-305.

Klein, G. deV., 1962, Triassic Sedimentation, Maritime Provinces, Canada, G.S.A. Bull. V. 73, p. 1127-1146.

Klein, G. deV., 1970, Depositional and Dispersal Synamics of Intertidal Sand Bars, J. Sed. Pet., V. 40, No. 4, p. 1095-1127.

Knight, R.J., 1977, Sediments, Bedforms and Hydraulics In A Macrotidal Environment, Cobequid Bay (Bay of Fundy), Nova Scotia. Unpublished Ph.D. Thesis, McMaster University.

Krinsley, D. et al., 1964, Transportation of Sand Grains Along the Atlantic Shore of Long Island, New York: An Application to Electron Microscopy, Marine Geology, 2 (1964), p. 100-120.

Krinsley, D., and Donahue, J., 1968, Environmental Interpretation of Sand Grain Surface Textures by Electron Microscopy, G.S.A. Bull., V. 79, p. 743-748.

Krinsley, D., and Donahue, J., 1968, Methods to Study Surface Textures of Sand Grains, A Discussion. Sed. 10 (1968), p. 217-221.

Krinsley, D., and Margolis, S., 1969, A Study of Quartz Sand Grain Surface Textures with the Scanning Electron Microscope, Trans. New York Acad. of Sci., Series II, V. 31, No. 5, p. 457-477.

Krinsley, D., and Smalley, I.J., 1972, Sand, Amer. Sci., V. 3, p. 286-291.

Krinsley, D., and Doornkamp, J.C., 1973, Atlas of Quartz Sand Surface Textures, Cambridge University Press, 1973.

Krinsley, D., Biscayne, P.E., and Turekian, K.K., 1973, Argentine Basin Sediment Sources as indicated by Quartz Surface Textures, J. of Sed. Pet., V. 43, No. 1, p. 251-257.

Krumbein, W.C., 1934, Size Frequency Distributions of Sediments, J. Sed. Pet., V. 4, p. 65-77.

Margolis, S.V., 1968, Electron Microscopy of Chemical Solution and Mechanical Abrasion Features on Quartz Sand Grains, Sed. Geol. 2 (1968), p. 243-266.

Margolis, S.V., and Kennet, J.P., 1971, Cenozoic Paleoglacial History of Antarctica Recorded in Sub-Antarctic Deep Sea Cores, Amer. J. Sci., V. 271, p. 1-35.

Margolis, S.V., and Krinsley, D.H., 1974, Processes of Formation and Environmental Occurance of Microfeatures on Detrital Quartz Grains, Am. J. Sci., V. 274, May, 1974, p. 449-464.

McManus, D.A., 1963, A Criticism of Certain Usage of the Phi-Notation, J. Sed. Pet., V. 33, No. 3, p. 670-674.

McWhirter, N., and McWhirter, R., (eds.), 1972, Guinness Book of Records, Nineteenth ed., Redwood Press Ltd., Enfield.

McQuivey, R.S., and Keefer, T.N., 1969, The Relation of Turbulence to Deposition of Magnetite over Ripples, U.S. Geol. Surv. Prof. Paper 650-B, p. 244-247.

Middleton, G.V., 1976, Hydraulic Interpretation of Sand Size Distributions, J. Geol., V. 84, p. 405-426.

Middleton, G.V., and Southard, J. B., 1977, Mechanics of Sediment Movement, S.E.P.M. Short Course Number Three.

Middleton, G.V., and Davis, P.M., 1979, Surface Textures and Rounding of Quartz Sand Grains on Intertidal Sand Bars, Bay of Fundy, Can. J. Earth Sci., V. 16, No. 11, p. 2071-2085.

Scholle, P.A., 1979, Constituents, Textures, Cements, and Porosities of Sandstones and Associated Rocks, A.A.P.G. Memoir 28.

Seward-Thompson, B.L., and Hails, J.R., 1973, An Appraisal of the Computation of Statistical Parameters in Grain Size Analysis, Sedimentology, V. 20, p. 161-169.

Shenk, P.E., 1975, A Regional Synthesis, Maritime Sediments, V. 11, p. 17-24.

Stepard, F.P., 1930, Fundian Faults or Fundian Glaciers, Geol. Soc. Amer. Bull., V. 41, p. 659-674.

Stepard, F.P., 1942, Origin of the Bay of Fundy, J. Geomorph., V. 5, p. 137-142.

Stieglitz, R.D., 1969, A Study of Freshwater Sand Grain Surfaces by Scanning Electron Microscopy, Proc. 12th Conf. Great Lakes, p. 351-356, Int. Assoc., Great Lakes Res.

Stieglitz, R.D., 1969, Surface Textures of Quartz and Heavy Mineral Grains From Freshwater Environments: An Application of Scanning Electron Microscopy, G.S.A. Bull., V. 80, p. 2091-2094.

Swift, D.J.P., and Lyall, A., 1968, Origin of the Bay of Fundy, and Interpretation from Sub-Bottom Profiles, Mar. Geol., V. 6, p. 331-343.

Wehrfritz, W., 1973, A Study of the Surface Textures of Intertidal Sand Grains with a Scanning Electron Microscope. Unpublished Tech. Memo 73-8, McMaster University, August, 1973.

White, J.R., and Williams, E.G., 1967, The nature of a Fluvial Process as Defined by Settling Velocities of Heavy and Light Minerals, J. Sed. Pet., V. 37, No. 2, p. 530-539.

Appendix 1

This appendix includes "V" pit densities and roundness values for each grain from sample SB-1. Where several values were calculated at a given magnification and sample area, only the mean value is shown. Grain roundness is given as: VA = Very Angular, A = Angular, SA = Subangular, SR = Subrounded, R = Rounded.

Grain Size Phi	Grain	10000X Magnification Sample Area Size $6.25\ \mu^2$	10000X Magnification Sample Area Size $25\ \mu^2$	5000X Magnification Sample Area Size $25\ \mu^2$	5000X Magnification Sample Area Size $100\ \mu^2$	Roundness
-1.0						
	2A	5.44	6.40	4.52	3.27	SR
-0.5						
	1A	4.21	3.65			A
	1B			3.28	2.68	SA
	2A	4.72	4.38			SA
	3B	6.08	5.12	3.96	2.99	SR
0.0						
	1B	3.36	2.60			SR
	1C			2.02	1.98	SA
	2A	3.20	2.92			SA
	2B	2.80	2.84	1.72	1.76	SA
	3A	2.40	2.48			SA
	3C	2.96	3.18	2.24	2.26	SR

Grain Size Phi	Grain	10000X Magnification Sample Area Size 6.25 μ^2	10000X Magnification Sample Area Size 25 μ^2	5000X Magnification Sample Area Size 25 μ^2	5000X Magnification Sample Area Size 100 μ^2	Roundness
0.0	4A	5.71	4.53			SR
	5A	3.52	3.50			SR
	5D	4.75	3.56			R
+0.5						
	1A	3.44	3.68	2.32	2.12	SA
	2A	3.76	3.46	2.06	2.19	SA
	2B	2.32	2.84	1.88	1.92	SR
	2D			1.86	1.30	R
	2E	2.96	3.14			SA
	3B	2.24	2.36	1.96	1.77	SR
	3D	4.32	3.56	2.18	1.99	SR
	3E	3.68	3.36	2.48	2.16	SA
	4A	4.00	3.88	3.04	2.76	SR
	4B	3.68	3.56	2.24	2.23	A
	4C	3.20	3.06	1.84	1.38	R
	5B	3.68	3.18	2.62	2.24	SA
	5C	3.28	3.00	2.00	1.76	SA
+1.0						
	1A	2.40	2.31			SA

Grain Size Phi	Grain	10000X Magnification Sample Area Size $6.25\ \mu^2$	10000X Magnification Sample Area Size $25\ \mu^2$	5000X Magnification Sample Area Size $25\ \mu^2$	5000X Magnification Sample Area Size $100\ \mu^2$	Roundness
+1.0	2A	3.04	2.44			A
	2B	2.08	2.22	1.64	1.55	SA
	2C	2.88	2.76	1.68	1.51	SR
	3A	2.40	3.12	1.54	1.55	R
	3D	2.48	2.36	1.04	1.07	SR
	3F	1.44	1.44	1.16	1.19	SR
	4A	2.08	1.61	1.48	1.51	R
	4C			2.52	1.70	SR
	4D	3.36	3.28			SA
	5A	2.88	2.48	1.08	1.14	A
	5B	2.29	2.39	1.95	1.50	SA
+1.5						
	1B	1.44	1.32	0.84	0.72	SA
	1C			0.72	0.71	SA
	1D			1.44	1.36	SA
	2A	1.6	2.4	1.20	1.12	SA
	2B	2.88	2.52			VA
	2D	2.24	1.74			SR
	2F			0.96	0.85	SR

Grain Size Phi	Grain	10000X Magnification Sample Area Size		5000X Magnification Sample Area Size		Roundness
		$6.25 \mu^2$	$25 \mu^2$	$25 \mu^2$	$100 \mu^2$	
+1.5	2G	3.04	2.16	1.68	1.28	SR
	3A			0.96	0.92	SA
	3C	2.24	2.00	1.32	1.07	SR
	3D	2.4	1.90	0.84	0.99	SR
	4A	2.72	3.16			R
+2.0						
	1A	1.76	1.84	0.68	0.74	SR
	1B	2.00	1.42			SR
	1D	4.80	4.36			SA
	1E	4.80	3.40	1.68	1.46	SA
	2B	1.92	1.28	0.92	0.83	SR
	2C			0.40	0.37	R
	2D	1.12	1.24			SA
	2E	2.00	2.46	1.40	1.37	SA
	3B	2.40	1.60	0.68	0.66	SR
	3C	1.44	1.16	0.96	0.84	SR

Appendix 2

This appendix includes all the cumulative weight percent values obtained by sieving the samples at half phi intervals.

Selma Bar

1) Samples from location SB-MIII.

SB-MIII Sample	Size (Phi) 0.0	0.5	1.0	1.5	2.0	2.5	3.0	3.5	4.0
d-2	0	0.03	1.56	23.16	66.94	86.72	96.19	99.05	99.68
c-2	0.04	0.11	1.41	21.42	69.52	89.59	97.17	99.38	99.83
b-2	0	0.04	0.42	10.09	48.17	78.47	94.90	98.86	99.58
a-2	0	0	0.06	3.80	34.99	74.01	93.96	98.80	99.57
2	0	0	0.09	4.51	30.28	67.51	93.14	99.03	99.70
2a	0	0	0.64	16.89	64.79	89.71	97.45	99.55	99.89
2b	0	0	0.06	5.69	45.77	83.28	96.44	99.33	99.78
2c	0	0	0.11	6.79	47.66	82.82	96.13	99.10	99.69
2d	0	0	0.09	6.86	48.85	81.86	95.41	98.89	99.59
2e	0	0	0.19	10.05	52.56	82.81	95.57	99.01	99.68
2f	0	0	0.44	13.55	59.56	86.39	96.21	99.00	99.64
2g	0	0	0.42	11.98	55.92	84.81	95.62	98.81	99.60
2h	0	0.01	0.65	16.28	60.30	83.77	95.41	98.81	99.54
2i	0	0.03	1.10	15.73	57.95	85.19	96.68	99.35	99.78

Samples from Selmah Bar (SB-1) and East Noel Bar (ENB)

	Size (Phi units)												
Sample	-2.0	-1.5	-1.0	-0.5	0.0	0.5	1.0	1.5	2.0	2.5	3.0	3.5	4.0
SB-1	1.09	2.80	6.85	10.22	13.79	20.00	41.08	69.63	87.26	97.95	99.54	99.90	99.99
ENB													
f-1	0	0	0	0	0	0	0.01	0.12	5.85	51.36	85.35	97.71	99.42
e-1	0	0	0	0	0.017	0.02	0.06	0.43	12.20	64.22	90.71	98.79	99.78
d-1	0	0	0	0	0.02	0.06	0.14	0.69	15.06	71.23	93.58	99.04	99.80
c-1	0	0	0.04	0.07	0.08	0.10	0.15	0.53	11.91	64.46	91.81	99.23	99.87
b-1	0	0	0	0	0.03	0.06	0.13	0.74	15.70	66.48	88.72	97.63	99.24
a-1	0	0	0.05	0.07	0.07	0.09	0.16	0.63	13.44	68.27	92.76	99.13	99.84
1	0	0	0.03	0.06	0.13	0.24	0.48	1.68	20.74	79.82	96.41	99.56	99.88
1b	0	0	0	0.06	0.11	0.20	0.41	1.56	21.75	81.33	97.32	99.71	99.91
1d	0	0	0	0	0.04	0.13	0.33	1.35	19.29	78.22	95.81	99.52	99.87
1f	0	0	0	0.01	0.07	0.16	0.41	1.26	16.95	72.97	94.05	99.19	99.78
1h	0	0.08	0.11	0.20	0.36	0.55	0.84	1.82	17.98	74.56	94.43	99.26	99.79
ij	0	0	0	0	0.03	0.09	0.19	0.61	11.99	62.97	90.41	98.45	99.61
1l	0	0.35	0.42	0.43	0.48	0.52	0.63	1.08	13.50	66.64	89.56	97.18	98.90
1n	0	0.49	0.49	0.51	0.53	0.54	0.56	0.75	7.85	53.20	85.26	97.31	99.35
1p	0	0	0	0	0.02	0.03	0.06	0.44	15.47	72.17	94.51	99.39	99.85